DOI:
10.1053/j.gastro.2018.08.023

Accepted Manuscript

Evidence of Chronic Allograft Injury in Liver Biopsies From Long-term Pediatric Recipients of Liver Transplants

Sandy Feng, John C. Bucuvalas, Anthony J. Demetris, Bryna E. Burrell, Katherine M. Spain, Sai Kanaparthi, John C. Magee, David Ikle, Andrew Lesniak, Juan J. Lozano, Estella M. Alonso, Robert A. Bray, Nancy E. Bridges, Edward Doo, Howard M. Gebel, Nitika A. Gupta, Ryan W. Himes, Annette M. Jackson, Steven J. Lobritto, George V. Mazariegos, Vicky L. Ng, Elizabeth B. Rand, Averell H. Sherker, Shikha Sundaram, Yumirle P. Turmelle, Alberto Sanchez-Fueyo

PII: S0016-5085(18)34888-1
DOI: 10.1053/j.gastro.2018.08.023
Reference: YGAST 62056

To appear in: *Gastroenterology*
Accepted Date: 8 August 2018

Please cite this article as: Feng S, Bucuvalas JC, Demetris AJ, Burrell BE, Spain KM, Kanaparthi S, Magee JC, Ikle D, Lesniak A, Lozano JJ, Alonso EM, Bray RA, Bridges NE, Doo E, Gebel HM, Gupta NA, Himes RW, Jackson AM, Lobritto SJ, Mazariegos GV, Ng VL, Rand EB, Sherker AH, Sundaram S, Turmelle YP, Sanchez-Fueyo A, Evidence of Chronic Allograft Injury in Liver Biopsies From Long-term Pediatric Recipients of Liver Transplants, *Gastroenterology* (2018), doi: 10.1053/j.gastro.2018.08.023.

Fonts, Arrows and Color Palette for Use

Use this font for large labels (Arial 20pt)

Use this font for small labels (Arial 16pt)

Use these arrows as needed

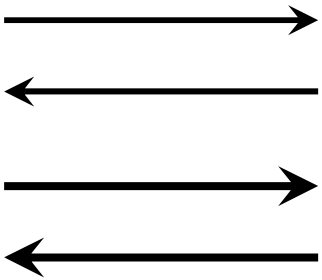

Selection of recommended colors

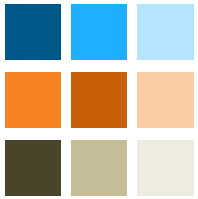

Subclinical Damage in Long-term Pediatric Liver Transplant Allografts

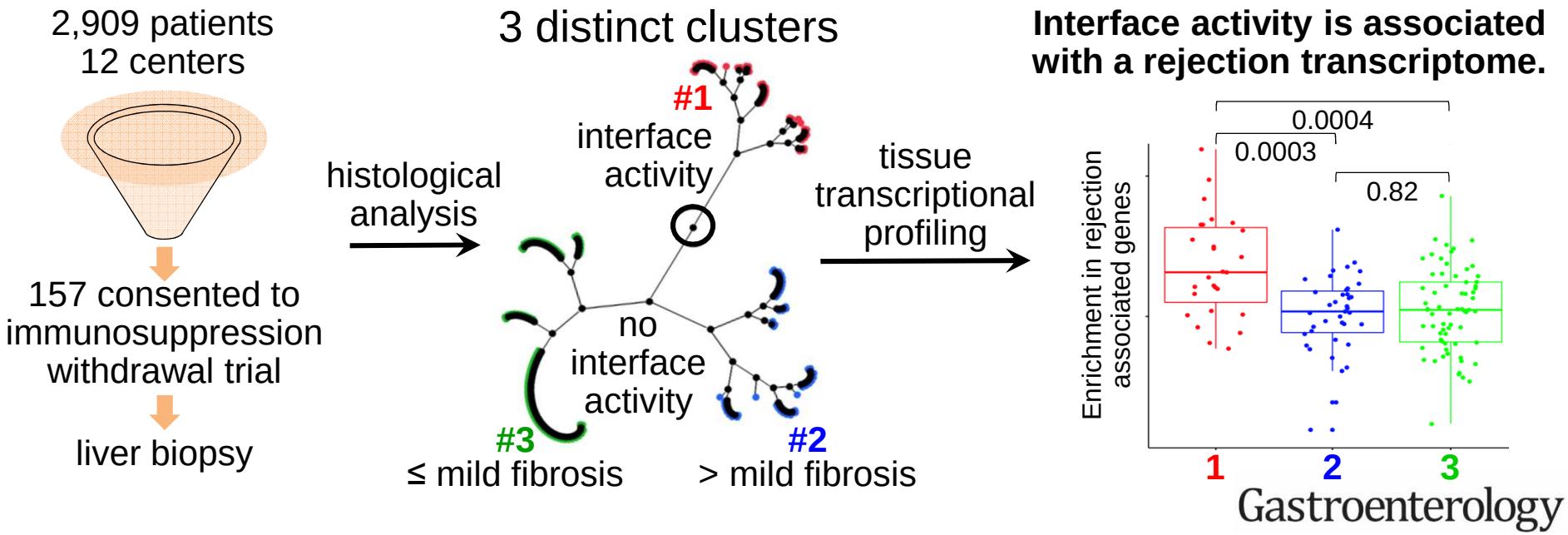

Evidence of Chronic Allograft Injury in Liver Biopsies From Long-term Pediatric Recipients of Liver Transplants

Sandy Feng,[1] John C. Bucuvalas,[2] Anthony J. Demetris,[3] Bryna E. Burrell,[4] Katherine M. Spain,[5] Sai Kanaparthi,[4] John C. Magee,[6] David Ikle,[5] Andrew Lesniak,[3] Juan J. Lozano,[7] Estella M. Alonso,[8] Robert A. Bray,[9] Nancy E. Bridges,[10] Edward Doo,[11] Howard M. Gebel,[9] Nitika A. Gupta,[12] Ryan W. Himes,[13] Annette M. Jackson,[14] Steven J. Lobritto,[15] George V. Mazariegos,[16] Vicky L. Ng,[17] Elizabeth B. Rand,[18] Averell H. Sherker,[8] Shikha Sundaram,[19] Yumirle P. Turmelle,[20] and Alberto Sanchez-Fueyo[21]

Short Title: Silent Graft Injury in Pediatric Liver Transplant Recipients

Corresponding Author:

Sandy Feng, MD, PhD

Professor of Surgery in Residence

University of California San Francisco

505 Parnassus Avenue

San Francisco, CA 94143-0780

Email: sandy.feng@ucsf.edu

Telephone: (415) 353-8725

Fax: (415) 353 8709

Author Affiliations

[1] Division of Transplantation, Department of Surgery, University of California San Francisco, San Francisco, CA; [2] Pediatric Liver Care Center, Cincinnati Children's Hospital Medical Center, Cincinnati, OH; [3] Department of Pathology, University of Pittsburgh, Pittsburgh, PA; [4] The Immune Tolerance Network, Bethesda, MD; [5] Rho, Inc., Chapel Hill, NC; [6] Section of Transplant Surgery, Department of Surgery, University of Michigan, Ann Arbor, MI; [7] Biomedical Research Center in Hepatic and Digestive Diseases, Carlos III Health Institute, Barcelona, Spain; [8] Siragusa Transplantation Center, Ann & Robert H. Lurie Children's Hospital of Chicago, Chicago, IL; [9] Department of Pathology, Emory University Hospital, Atlanta, GA; [10] Transplantation Branch; Division of Allergy, Immunology, and Transplantation, National Institute of Allergy and Infectious Diseases, Rockville, MD; [11] Division of Digestive Diseases and Nutrition, National Institute of Diabetes and Digestive and Kidney Diseases, Bethesda, MD; Department of Pathology, Emory University Hospital, Atlanta, GA; [12] Division of Pediatric Gastroenterology, Hepatology and Nutrition, Department of Pediatrics, Emory University School of Medicine, Atlanta, GA; [13] Section of Gastroenterology, Hepatology, and Nutrition, Texas Children's Hospital, Houston, TX; [14] Division of Immunogenetics and Transplantation Immunology, Department of Medicine, Johns Hopkins University, Baltimore, MD; [15] Center for Liver Diseases and Transplantation, Department of Surgery, Columbia University Medical Center, New York, NY; [16] Hillman Center for Pediatric Transplantation, Children's Hospital of Pittsburgh of UPMC, Pittsburgh, PA; [17] Division of Pediatric Gastroenterology, Hepatology and Nutrition, Transplant and Regenerative Medicine Center, Toronto, Ontario, Canada; [18] Liver Transplant Program, The Children's Hospital of Pennsylvania, Philadelphia, PA; [19] Division of Gastroenterology, Hepatology, and Nutrition, Children's Hospital Colorado, University of Colorado School of Medicine, Aurora, CO; [20] Division of Gastroenterology, Hepatology, and Nutrition, St. Louis Children's Hospital, St. Louis, MO; and [21] Institute of Liver Studies; King's College, London; London, United Kingdom

Author Roles and Contributions

	Concept Design	Data Acquisition	Analysis/Data Interpretation	Manuscript Drafting	Critical Revision	Statistical Analysis	Obtained Funding	Technical Support	Material Support	Study Supervision
Feng	X	X	X	X	X	X	X			X
Bucuvalas	X	X	X	X	X	X	X			X
Demetris	X	X	X	X	X	X				
Burrell			X	X	X			X		
Spain			X	X	X	X		X		
Kanaparthi			X	X	X	X		X		
Magee	X	X	X	X	X					
Ikle	X		X	X	X	X				
Lesniak			X	X	X	X		X		
Lozano			X		X	X		X	X	
Alonso	X	X			X					
Bray		X	X		X					
Bridges	X				X					X
Doo	X				X					X
Gebel		X	X		X					
Gupta	X	X			X					
Himes	X	X			X					
Jackson		X	X		X			X	X	
Lobritto	X	X			X					
Mazariegos	X	X	X		X					
Ng	X	X			X					
Rand	X	X			X					
Sherker	X				X					X
Sundaram	X	X			X					
Turmelle	X	X			X					
Sanchez-Fueyo	X	X	X	X	X	X				

Abbreviations used in this manuscript:

ABMR	antibody mediated rejection
ALT	alanine aminotransferase
ANA	anti-nuclear antibody
ASMA	anti-smooth muscle antibody
APC	antigen presenting cell
AT1R	angiotensin 2 type 1 receptor
BAT	B cell specific transcripts
DSA	donor specific HLA antibody
ETAR	endothelin
FDR	false discovery rate
GGT	gamma-glutamyl transferase
GRIT1	IFN-γ dependent rejection-associated transcripts
IgG	immunoglobulin
IGT	immunoglobulin associated transcripts
KEGG	Kyoto Encyclopedia of Genes and Genomes
LAFSc	liver allograft fibrosis score
LIMMA	linear models for microarray analyses
MCAT	mast cell associated transcripts
MFI	mean fluorescence intensity
QCAT	cytotoxic T lymphocyte associated transcripts
Qdot	quantum dot
SAM	significant analysis of microarray
SD	standard deviation

SMA	smooth muscle actin
TCB	T cell specific transcripts
TCMR	T cell mediated rejection
WGCNA	whole genome correlated network analysis
WSI	whole slide images

ACKNOWLEDGEMENTS

The authors would like to extend their appreciation towards all of the patients and their families that participated in this study. We wish to thank the following: Sharon Blaschka, Crystal Lala, Kalpana Harish, Allan Kirk, Allison Priore, iWITH co-investigators and research coordinators, and the staff at all iWITH core laboratories for their contributions. We acknowledge the support received by the National Institutes of Health's (NIH) National Center for Advancing Translational Sciences from the following institutions: University of California, San Francisco, San Francisco, CA; Ann & Robert H. Lurie Children's Hospital of Chicago, Chicago, IL; Columbia University, New York, NY; Cincinnati Children's Hospital, Cincinnati, OH; Children's Hospital Colorado, Denver, CO; The Children's Hospital of Philadelphia, Philadelphia, PA; St. Louis Children's Hospital, St. Louis, MO and Emory University School of Medicine, Atlanta, GA.

CONFLICTS OF INTEREST

A.M.J. is on the speakers' bureau and receives honoraria from One Lambda. The authors disclose no other conflicts.

FUNDING

This research was primarily supported by U01-AI-100807 awarded by the National Institute of Allergy and Infectious Diseases (NIAID) and the National Institute for Diabetes and Digestive and Kidney Diseases. In addition, the research was also performed as a project of the Clinical Trials in Organ Transplantation in Children (U01-AI-104347), a collaborative clinical research project headquartered at NIAID and as a project of the Immune Tolerance Network (UM1AI109565), an international clinical research consortium headquartered at the Benaroya Research Institute and supported by NIAID. The content is solely the responsibility of the authors and does not necessarily represent the official views of the NIH.

ABSTRACT

Background and Aim: A substantial proportion of pediatric liver transplant recipients develop subclinical chronic allograft injury. We studied whether there are distinct patterns of injury based on histopathology features and identified associated immunological profiles.

Methods: We conducted a cross-sectional study of 157 stable, long-term pediatric recipients of transplanted livers (70 boys; less than 6 years old; mean 8.9±3.46 years after liver transplant) who underwent liver biopsy analysis from August 13, 2012 through May 1, 2014. Subjects received livers from a living or deceased donor and had normal results from liver tests for more than 4 years after receiving transplant. Liver biopsies were scored by a central pathologist; an unsupervised hierarchical cluster analysis of histologic features was used to sort biopsies into 3 clusters. We conducted transcriptional and cytometric analyses of liver tissue samples and performed a systems biology analysis that incorporated clinical, serologic, histologic, and transcriptional data.

Results: The mean level of alanine aminotransferase in subjects was 27.6±14.57 U/L and the mean level of gamma-glutamyl transferase was 17.4±7.93 U/L. Cluster 1 was characterized by interface activity (n=34), cluster 2 was characterized by periportal or perivenular fibrosis without interface activity (n=45), and cluster 3 had neither feature (n=78). We identified a module of genes whose expression correlated with levels of alanine aminotransferase, class II donor-specific antibody, portal inflammation, interface activity, perivenular inflammation, portal and perivenular fibrosis, and cluster assignment. The module was enriched in genes that regulate T-cell mediated rejection (TCMR) of liver and other transplanted organs. Functional pathway analysis revealed over-representation of TCMR gene sets for cluster 1 but not clusters 2 or 3.

Conclusion: In an analysis of biopsies from an apparently homogeneous group of stable, long-term pediatric liver transplant recipients with consistently normal results from liver tests, we found evidence of chronic graft injury (inflammation and/or fibrosis). Biopsies with interface activity had a gene expression pattern associated with TCMR.

Key words: ALT, DSA, immune response, prognostic factor

There are now thousands of long-term pediatric liver transplant recipients who apparently enjoy excellent health with no biochemical evidence of allograft injury. While this success is worthy of celebration, it has also generated new questions as to how best to care for these young patients. The goal of securing excellent health over many decades requires constant consideration of optimal immunosuppression to ensure efficacy while minimizing toxicity. The risks associated with low dose but chronic immunosuppression have been described[1-7] leading to substantial efforts directed at drug minimization. Indeed, several prospective, multicenter clinical trials have reported complete discontinuation of immunosuppression without progressive allograft damage in select adult and pediatric recipients.[8-11] In contrast, multiple centers around the world have reported that liver allografts of patients maintained on standard of care immunosuppression frequently harbor *subclinical* inflammation and/or fibrosis.[12-18] Moreover, the prevalence and severity of allograft histopathology has been reported to increase over time such that, 10 years after transplant, normal histology may be present in only 30% of patients while bridging fibrosis or cirrhosis may approach 60%.[13, 15, 16] Together, these reports have suggested that the observed abnormalities reflect an active and ongoing immune response, implicating chronic but imprecisely-defined immune mechanisms.[13, 16, 19-24] Consequently, clinicians have been left with a challenging quandary when managing stable patients with consistently normal results of liver tests on modest immunosuppression doses: reduce immunosuppression at the risk of exacerbating silent, immune-mediated allograft injury, stay the course with uncertainty as to whether dosing is appropriate, or escalate immunosuppression unnecessarily, increasing the risk of known toxicities.

Based on the contradictory literature regarding optimal immunosuppression for pediatric liver transplant recipients who appear stable by clinical and biochemical criteria, we hypothesized that these patients are not homogeneous but would sort into distinct histopathological phenotypes reflecting

specific mechanisms of chronic graft injury. The aim of this study was to identify these phenotypes and elucidate their associated immunologic profiles. We utilized prospectively collected data and biospecimens at the time of screening for participation in iWITH (NCT01638559), a prospective, multicenter, North American trial of immunosuppression withdrawal for stable pediatric liver transplant recipients. We believe that a clear description and plausible explanation of histopathological phenotypes can have an immediate impact on clinical decision-making and inform the future design of rational interventions to maximize allograft longevity.

METHODS

Study Design

We carried out a cross sectional study using data (donor, recipient and transplant) and biospecimens collected at the time of liver biopsy, the final eligibility assessment for participation in iWITH (NCT01638559), an immunosuppression withdrawal trial conducted at 12 pediatric liver transplant centers in North America (Table 1). The analysis population included all 157 patients who provided age-appropriate informed assent and consent (parent/legal guardian) to iWITH and underwent a liver biopsy between August 13, 2012 and May 1, 2014.

Subjects: Key Inclusion/Exclusion Criteria

Subjects (<18 years) were ≥4 years after primary living or deceased donor liver transplantation for non-viral and non-autoimmune liver disease at ≤6 years of age who underwent screening liver biopsy for iWITH. Participants were required to have alanine aminotransferase (ALT) and gamma-glutamyl transferase (GGT) consistently less than 50 IU/L based on medical record review by the site principal

investigator and to be stably maintained on calcineurin inhibitor monotherapy without rejection during the preceding two years (Figure 1).

Routine Histology, C4d Scoring, Multiplex Quantum Dot (Qdot) Immunolabelling, and Automated Image Analysis

High resolution 40Xwhole slide images (WSI) of formalin-fixed, paraffin-embedded, H&E and Masson's trichrome-stained 4μm tissue sections of eligibility liver biopsies were prospectively scored for 42 histopathologic criteria by a central pathologist without knowledge of any clinical or serological data other than the date of transplantation and original disease. Fibrosis was assessed in several ways: Ishak stage (0-6), individual compartmental scores (periportal, sinusoidal, and perivenular; 0-3 each), 3-compartment sum (0-9) known as the liver allograft fibrosis score (LAFSc)[16] and quantitatively using a combination of pixel area morphometry and/or tissue tethered cytometry[25] after Qdot multiplex panel immunostaining [trichrome and smooth muscle actin (SMA) staining] (Supplementary Figure 1). C4d deposition was evaluated on frozen biopsies using indirect immunofluorescence staining for C4d (mouse monoclonal Quidel, San Diego, CA, 1:50) in distinct vascular endothelial compartments and surrounding stroma (portal vein and capillary, portal stroma, hepatic artery, sinusoid, central vein and stroma); each was separately scored (0=none; 1=minimal; 2=focal; 3=diffuse) and summed for a total C4d score (0-18). Batched slide sets were multiplex-stained and evaluated as described in the Supplementary Methods.

Derivation of Histopathological clusters

Subjects' histologic scores were classified by an unsupervised hierarchical cluster analysis using Ward's minimum-variance method with standardized data points. Ten features were initially considered, but only 5 exhibited sufficient variability to be considered further: interface activity, perivenular fibrosis, fibrosis stage, lobular inflammation, and portal inflammation. Subjects were categorized into 3 clusters

using 3, 4 and 5 variable models and results were compared to determine the best classification model using 3 criteria, R square, cubic clustering, and pseudo-F statistic, to determine goodness of fit.

Analysis of liver tissue gene expression data

Affymetrix U219 microarray data was available from 133 of the 157 liver biopsies and analyses were batched to minimize bias. Differential expression was computed employing Significant Analysis of Microarray (SAM)[26]and expressed as False Discovery Rate (FDR). We used Weighted Gene Correlation Network Analysis (WGCNA; software package available from R[28])[27] to identify the key biological networks associated with the demographic, clinical serological and histological features of the study subjects. This is a widely used, unsupervised, and exploratory data mining technique that reduces the multi-dimensionality of the gene expression dataset by defining modules of co-expressed genes and integrates external variables (e.g. clinical or histological traits) by establishing weighted correlations with the gene modules. Validation gene expression experiments for a set of 800 pre-defined genes were conducted on 148 RNA samples utilizing a Nanostring nCounter platform. A detailed description of the gene expression experiments is provided in the Supplementary Methods.

Autoantibody assessment

Samples isolated from plasma or serum collection tubes were assayed for quantitative serum immunoglobulin G (IgG), α-nuclear antibodies (ANA), α-smooth muscle antibodies (ASMA), α-angiotensin II type 1 receptor (AT1R) antibody and α-endothelin type A receptor (ETAR) antibody. (EIA-AT1RX/EIA-ETAR, One Lambda, Canoga Park, CA).

HLA typing and alloantibody characterization

HLA typing data was retrieved from United Network for Organ Sharing for 106 deceased and 24 living

donors. HLA typing was performed by SSP or SSO (One Lambda, Canoga Park, CA) for 20 living donors and 154 recipients. HLA typing data was unavailable for 7 donors (4 deceased; 3 living) and 3 recipients. HLA mismatch data is presented in Supplementary Table 1.

Screening and specificity analysis for donor-specific HLA antibody (DSA) against HLA antigens was determined using FlowPRA®Screening and LabScreen® Single Antigen™ (One Lambda, Canoga Park, CA). FlowPRA® was acquired on a FACSCanto II (Becton-Dickinson, San Jose CA.) and Single Antigen™ bead assessments were performed on the LABScan 200 instrument (Luminex Corp. Austin, TX). Samples with sufficient volume were also tested using C1qScreen™ (One Lambda Inc., Canoga Park, CA, USA) acquired on a LabScan3D instrument (Luminex Corp., Austin, TX). HLA pattern analysis and bead mean fluorescence intensity (MFI) >2000 for LabScreen® and >5000 for C1qScreen™ determined positivity. Only class II DSA data are presented as the preponderance of literature indicates their primacy in chronic allograft damage.[22, 28, 29] HLA-DRB1-DQB1-DQA1 linkage-disequilibrium data was used to assign donor specificity for HLA-DQ antibodies for subjects with limited donor HLA-DQ typing.

Statistical Analysis

Descriptive statistics including mean, standard deviation (SD), and quartiles were determined for continuous variables and frequencies and percentages were determined for categorical variables. Comparisons of categorical variables between two groups used the Fisher exact test while comparisons of continuous variables with two groups used the two-sample t-test. Comparisons of continuous variables with more than two groups used ANOVA.

Multivariable logistic regression analyses were used to study associations between histological features, C4d scores and serological profiles. Univariable and multivariable logistic regression analyses were used to identify selected predictors of subjects' histologic cluster assignment among clinical and serologic

factors along with their interactions. Small amounts of missing data in risk factors were accommodated in the multivariable analyses by case-wise deletion. Significant predictors at the 0.10 level in the univariable analyses were included in the multivariable models. Backwards variable elimination using 0.10 as the threshold for retention resulted in the final multivariable model. The model was internally validated using 1000 bootstrapped resamples to produce an optimism-adjusted area under the curve. Statistical significance was set at an alpha level of 0.05. All statistical analyses were performed using SAS software (version 9.4, SAS Institute, Inc., Cary, NC, USA). All authors had access to the study data and reviewed and approved the final manuscript.

RESULTS

Characteristics of enrolled subjects

Subjects (79 boys; 84% white) were a mean (SD) 1.8 (1.70) years old at transplant and 10.7 (3.50) years old at enrollment (Table 1). They underwent living (n=47; 30%) or deceased [whole n=73 (47%); partial n=37 (24%)] donor liver transplant predominantly for biliary atresia (55%). A modest proportion received induction immunosuppression (n=21; 13%). At enrollment, all were on calcineurin inhibitor monotherapy with mean (SD) ALT of 27.6 (14.57) U/L and GGT of 17.4 (7.93) U/L.

Inflammation, fibrosis, and C4d scores for 157 eligibility biopsies

The 157 eligibility biopsies were assessed for necroinflammatory activity and fibrosis (Figures 2A and 2B). Lymphocytic inflammation was common in the portal/periportal area (59% mild; 5% moderate) but less so in the perivenular (17% mild) area. A minority showed interface activity (21% mild; 1% moderate), lobular (23% mild; 1% moderate) or perivenular inflammation (17% mild). As expected, inflammation and fibrosis typically occurred together and were spatially associated. Biopsies with portal inflammation and interface activity had higher Ishak fibrosis stages while biopsies with perivenular

inflammation had higher perivenular fibrosis scores. However, fibrosis and inflammation were occasionally disconnected: some biopsies showed mild or moderate portal or perivenular fibrosis but no inflammation while others showed mild portal inflammation without interface activity and low Ishak fibrosis stage and LAFSc.

C4d scores, total and by compartment, are shown in Supplementary Figures 2A and 2B. The two stromal compartments, portal and perivenular, were most frequently positive. Portal stromal staining was associated with portal inflammation (p=0.03); perivenular stromal staining was associated with perivenular inflammation (p=0.009) (Supplementary Table 2). The distribution and intensity of microvascular endothelial cell C4d staining followed both HLA class II target antigen expression[30-32] and blood flow: portal capillaries > sinusoids > central vein. No other significant associations with routine histopathology findings were detected.

Auto- and alloantibody profiles of subjects

ANA and ASMA were positive in 26% (34/133) and 4% (5/133), respectively; mean (SD) IgG was 701.0 (194.95) mg/dL (Table 1; Supplementary Figure 3). Most subjects were positive for α-AT1R and α-ETAR antibodies (68.1% and 66.4%, respectively) with mean (SD) concentrations of 35.9 (21.49) and 35.2 (21.39) U/mL, respectively. Subjects positive for ANA were older at study entry with a longer interval since transplant. In contrast, those positive for α-AT1R and α-ETAR antibodies were younger at time of study entry with a shorter interval since transplant. Associations between clinical characteristics and autoantibody profile are shown in Supplementary Table 3A.

For class II DSA, 80 of 144 (55.6%) tested subjects were positive with mean (SD) MFI sum of 26,699 (16,674). Forty-two subjects had a single class II DSA, 28 had 2 class II DSAs, and 10 had 3 or more class

II DSAs (Table 1). Among the 130 class II DSAs identified, 38.5% had MFI >20,000 and 68.5% had specificity against DQ antigens. Thirty-seven of 80 (46.2%) subjects had at least one class II DSA with MFI >20,000 (data not shown); eight additional subjects with >1 DSA, had a DSA sum >20,000 MFI (data not shown). Finally, among the 80 subjects with class II DSA, 61 subjects had sufficient serum to test complement binding capacity. The majority (78.7%) tested positive, with mean C1q MFI >20,000; data not shown). Notably, no associations were identified between class II DSA parameters and clinical characteristics including age at transplant or study entry, interval since transplant, living or deceased donor recipient, or history of previous rejection (Supplementary Table 3B).

Associations between serological profiles, histological features, and C4d scores

Autoantibody parameters (quantitative IgG, ANA, ASMA, α-AT1R, and α-ETAR) in isolation did not show any association with either histological features or C4d scores. For analyses of class II DSA, we selected the sum of class II DSA MFI as the representative variable after testing positive/negative, maximum, and sum. A model including all serological variables confirmed the strong and dominant association between class II DSA MFI sum >20,000 and histological features as well as C4d scores (Supplementary Table 4). Compared to those with no class II DSA, those with class II DSA MFI sum >20,000 were at increased risk of higher Ishak fibrosis stage (OR 4.53; 95% CI 1.78-11.53; p=0.001), portal inflammation grade (OR 3.59; 95% CI 1.30-9.93; p=0.01), and C4d scores [portal capillary (OR 5.11; 95% CI 1.98-13.20; p<0.001), sinusoidal (OR 4.40; 95% CI 1.49-12.98; p=0.007; total (OR 4.73; 95% CI 1.95-11.48; p<0.001)].

157 biopsies sort into three distinct histopathological clusters

An unsupervised hierarchical cluster analysis identified three clusters based on three histological features (Figure 3). Cluster 1 (n=34) was defined by portal inflammation with interface activity, often

associated with variable degrees of fibrosis; cluster 2 (n=45) was characterized by significant Ishak and/or perivenular fibrosis but without interface activity; cluster 3 (n=78) were near normal, exhibiting neither interface activity nor significant fibrosis (Figure 3A). As evident in the constellation plot, cluster 1 clearly diverges from clusters 2 and 3 (Figure 3B). Given the reported association of DSA with chronic graft injury, we compared the prevalence of class II DSA among the clusters. When compared to cluster 2 and 3, a greater proportion of subjects in cluster 1 had class II DSA. The mean class II DSA MFI was higher in cluster 1 versus cluster 2 or 3. Moreover, a higher percentage of subjects in cluster 1, compared to clusters 2 and 3, had class II DSA MFI maximum >20,000 and class II DSA MFI sum >20,000 (Supplementary Figures 4A and 4B).

Quantitative determination of fibrosis, APCs, leukocytes, and APC: leukocyte pairings

Differences among the three histopathological clusters were next explored utilizing immunohistochemical and multiplex staining. Fibrosis severity, as quantified by both trichrome and SMA staining area, showed the expected trend among clusters (clusters 1 and 2 > cluster 3), but the differences were not statistically significant (data not shown). Cell counts within virtual antigen-presenting foci, which largely correspond to portal tracts (Methods; Figure 4A-C), readily distinguished the clusters. APCs (CD34-/CD45-/class II+), leukocytes (CD34-/CD45+(high)/class II+/-), and APC-leukocyte pairings, defined as an APC within 5 microns of a leukocyte, were quantified and compared. The number of APCs was significantly higher in clusters 1 and 2 compared to cluster 3 (Figure 4D). Total leukocyte counts were distinctly higher in cluster 1 but similar in clusters 2 and 3 (Figure 4E). The number of APC-leukocyte pairings differed among clusters, being highest in cluster 1 and lowest in cluster 3 (Figure 4F). Analyses over the total biopsy area, as opposed to the virtual antigen-presenting foci, showed less significant differences among the clusters (data not shown).

The histopathological features defining the three clusters are associated with a distinct module of co-expressed genes

To further identify the biological underpinnings of the subclinical histological and immunohistochemical abnormalities, we conducted whole genome transcriptional analysis of the liver tissue samples and applied WGCNA to identify modules of co-expressed genes that were correlated with demographic, clinical, serological and histological traits of interest. Out of the thirty-three distinct modules identified, one module comprising 194 genes, which we will refer to as the "salmon" module (Figure 5A; black arrow) showed significant correlation with cluster assignment, class II DSA, interface activity, Ishak fibrosis stage, portal inflammation, perivenular fibrosis, perivenular inflammation, serum ALT and, importantly, was not influenced by clinical confounders such as recipient age or time after transplant. This module of 194 genes (Supplementary Table 5) was enriched in pathways related to cytokine-cytokine receptors, chemokines, and allograft rejection, among others (Figure 5B). Moreover, 50 of the 194 genes had been previously described as being associated with T cell mediated rejection (TCMR) in microarray studies involving liver, kidney, lung, or heart transplantation (e.g. *CXCL9, CXCL10, HLA-DOB, CD3E, GZMB, PRF1, CD74*).[33-35] The overall transcript levels of this selected gene module across the whole liver tissue microarray data set significantly correlated with the LAFSc, suggesting a potential pathogenic role of these genes in liver allograft fibrosis (Figure 5C).

Transcriptional pathways involved in TCMR differentiate cluster 1 from clusters 2 and 3

To better understand the differences among the three histological clusters we conducted pairwise comparisons of their transcriptomes. Cluster 1 significantly differed from cluster 3 and, to a lesser degree, from cluster 2. In contrast, clusters 2 and 3 only showed minimal transcriptional differences (Figure 5D). These results and, in particular, the lack of significant differences in pro-inflammatory gene

expression between clusters 2 and 3 were confirmed on a Nanostring platform (Supplementary Figure 5 and Supplementary Tables 6A-C).

To identify the pathways associated with the differential gene expression between cluster 1 and clusters 2 and 3, we conducted functional pairwise analysis employing the QuSAGE method on a set of transcriptional pathways known to be involved in allograft immunopathogenesis across a variety of clinical and animal transplant settings. As a relevant control, we also included a 13-gene signature previously described as highly specific for TCMR in stable liver recipients undergoing immunosuppression withdrawal (Supplementary Table 7).[33] The liver rejection gene set was significantly associated with cluster 1 but not clusters 2 or 3. In addition, the following gene sets known to be involved in TCMR across a variety of clinical and experimental settings were also over-represented in cluster 1: *GRIT1* (IFN-γ dependent rejection-associated transcripts), *QCAT* (cytotoxic T lymphocyte associated transcripts), *TCB* (T cell specific transcripts), and *BAT* (B cell specific transcripts). Cluster 1 was also significantly enriched in the *IGT* gene set (immunoglobulin associated transcripts) as compared to clusters 2 and 3, and in the *MCAT* gene set (mast cell associated transcripts) as compared to cluster 3, both of which are known be associated with allograft fibrosis but not with rejection.[35] *IGT* was the only gene set over-represented in cluster 2 as compared to cluster 3 (Figure 5E).

We conducted a more extensive pathway analysis to better delineate the functional differences between cluster 2 and 3. The two clusters significantly differed in the over-representation of canonical pathways involved in fibrogenesis. In addition, cluster 2 was significantly enriched in a gene set specific for stellate cells whose expression has been associated with survival in non-transplanted patients with chronic liver disease[36]. In contrast, only minimal differences in inflammatory canonical pathways between the two clusters were noted (Supplementary Table 8).

To explore the impact of circulating class II DSA on the molecular profile of the liver allograft, we employed the Nanostring dataset to compute the liver gene expression differences between class II DSA positive versus negative individuals across the study cohort (Supplementary Table 9). The results greatly overlapped with the expression differences between cluster 1 and the other two clusters, likely reflecting the different prevalence of class II DSA among the three clusters. However, after fitting a linear model incorporating CD45+ cells to account for the imbalance in the degree of inflammatory infiltrate, we identified CCL18 and CXCL9 as transcriptional markers independently associated with class II DSA (FDR 0.0007 and 0.009, respectively).

ALT and MFI sum of class II DSA MFI >20,000 independently predict assignment into cluster 1

Finally, the mechanistic insight suggesting that subjects in cluster 1 are experiencing alloimmune graft injury motivated us to utilize logistic regression analyses to identify clinical and/or serological risk factors (Table 2). Univariable models identified deceased donor (OR 4.03; 95% CI 1.33-12.20; p=0.01), non-biliary atresia transplant indication (OR 2.38; 95% CI 1.08-5.26; p=0.03), decreased time between transplant and eligibility biopsy (OR 0.88 per year increment; 95% CI 0.78-0.99; p=0.03) and increased ALT (OR 1.06 per 1 IU/L increment; 95% CI 1.02-1.11; p=0.009) as associated with assignment into cluster 1 versus clusters 2 and 3. ANA and ASMA positivity were not associated with cluster 1 assignment but both α-AT1R (OR 1.03; 95% CI 1.01-1.05; p=0.01) and α-ETAR antibodies (OR 1.03; 95% CI 1.00-1.05; p=0.02) were associated with cluster 1 assignment. Class II DSA presence (OR 2.90; 95% CI 1.14-7.34; p=0.02) was also associated with assignment into cluster 1. The association was stronger when class II DSA MFI sum was >20,000 (OR 4.49; 95% CI 1.67-12.14; p=0.003) and strongest when class II DSA maximum was >20,000 (OR 5.55; 95% CI 2.00-15.44; p=0.001). We selected to use the sum of class II DSA MFI as the class II DSA variable. The final multivariable model shows that two factors, ALT

(OR 1.07 per U/L; 95% CI 1.02-1.13; p=0.01) and the sum of class II DSA MFI >20,000 (OR 5.11; 95% CI 1.82-14.41; p=0.002), were independently associated with assignment into cluster 1 versus 2 and 3 (Table 2).

DISCUSSION

Long-term sustainability of allograft and patient health is the primary challenge facing the liver transplant community. This challenge is undoubtedly the lengthiest and steepest for pediatric recipients. To address this challenge, we conducted a cross-sectional study of well-characterized, stable liver transplant recipients who had consented to enter a trial of complete immunosuppression withdrawal. As hypothesized, we were able to define, among this clinically homogeneous cohort, three distinct histopathological clusters, differentiated by the presence and severity of interface activity and/or fibrosis. To explore potential mechanism(s) underlying the distinctions among the clusters, we employed an unsupervised systems biology approach to analyze the liver tissue transcriptional patterns associated with clinical, serological, and histological features. This strategy allowed an unbiased assessment of the important parameters influencing the expression profiles as well as the identification of potential confounders. A module of co-expressed genes dominated by transcripts strongly associated with rejection[34, 35] was significantly correlated with class II DSA, interface activity, and fibrosis. Direct comparisons between clusters revealed that rejection-associated transcripts were predominantly increased in cluster 1, the cluster characterized by interface activity. This finding was confirmed at the functional pathway level: we showed that IFN-γ-regulated gene signatures known to be associated with TCMR in liver, kidney, and heart transplantation were significantly enriched.[35, 37] The suggestion that interface activity may reflect subclinical rejection has implications for the optimal management of immunosuppression for this subset of patients that merits future testing. The approach is clearly different from efforts to withdraw immunosuppression for those without interface activity who

ultimately participated in the iWITH trial. Our description of distinct histopathological phenotypes and provision of their associated molecular patterns is a necessary step towards the personalization of immunosuppression management necessary to simultaneously optimize patient and graft health and longevity.

After liver transplantation, it is understood that the inflammatory damage of TCMR is orchestrated by effector T cells engaging alloantigen-bearing APCs and parenchymal cells, preferentially in the portal areas.[31] We found that the transcript levels of the set of 194 co-expressed genes directly and significantly correlated with the magnitude of leukocyte infiltration. Furthermore, liver biopsies from cluster 1 exhibited the highest number of APC-leukocyte pairings – leukocytes in close proximity to, and potentially interacting with, APCs. Although cluster 1 subjects also had the highest prevalence of class II DSA, we did not observe a significant enrichment in intra-graft endothelial or natural killer cell related gene signatures, which have been described as selective for antibody-mediated rejection (ABMR) in kidney and heart transplantation.[38, 39] The lack of up-regulation of classic ABMR-specific signatures strongly suggests that endothelial damage is not the primary pathogenic feature of the inflammatory changes observed in cluster 1 biopsies but does not exclude the involvement of DSA in immunopathogenesis. First, liver, compared to kidney and heart, allografts respond differently to DSA. Moreover, the histological features of chronic ABMR in liver transplantation remain incompletely defined.[31] As a result, liver-specific transcriptional signatures discriminating chronic ABMR from TCMR cannot be derived. Second, data from experimental animal models indicate that, in addition to their capacity to induce immunopathology by binding HLA molecules in the endothelium and activating complement and natural killer cells, alloantibodies can promote allograft rejection by an alternative mechanism that enhances the expansion and effector function of donor-specific T cells.[40] In support of a link between humoral sensitization and anti-donor T cell mediated responses, recent data from kidney

transplant patients with chronic ABMR[41] demonstrate that the magnitude of indirectly-primed CD4+ T cell responses (i.e. T cell responses elicited by recipient APCs presenting peptide fragments of donor graft antigens) correlates with the progression of kidney allograft dysfunction. Third, our observation that class II DSA was associated with expression of T cell chemokines such as CCL8 and CXCL9, after adjusting for the magnitude of inflammation, suggests a contributory role of class II DSA to the development of liver T cell infiltration. Taken together, these results indicate that patients with subclinical histological abnormalities that include interface activity (cluster 1) constitute a distinct phenotype that recapitulates the molecular mechanisms described in allograft rejection. Late subclinical histopathological abnormalities are prevalent in many different solid organ allografts and contribute to long-term allograft structural decline.[13, 19-23, 28, 29, 42-48] Whether, in liver transplantation, this is exclusively a T cell mediated process, or, more likely, a mixed process influenced by both humoral sensitization and T cell alloreactivity cannot as yet be determined.

In contrast to the interface activity characteristics of cluster 1, the pathogenesis of cluster 2 lesions, periportal and/or perivenular fibrosis without inflammation, remains more difficult to elucidate. There were only subtle transcriptional differences between clusters 2 and 3 in pro-inflammatory and rejection gene sets. Although cluster 2 compared to cluster 3 biopsies exhibited increased numbers of APCs and APC-leukocyte pairings, the differences were smaller than those between clusters 1 and 3. These small differences could reflect fibrotic changes or, alternatively, spatial or temporal sampling issues. Nevertheless, in sum, our data suggest that an active alloimmune response may not be the basis for the separation of cluster 2 from 3. Further research is necessary to determine the mechanism(s) underlying the “bland” fibrosis characteristic of cluster 2.

While this study is the product of a comprehensive mechanistic effort, there remain limitations. First and foremost, the liver biopsies were from a highly selected subset of pediatric liver transplant recipients. The prospective application of extensive inclusion/exclusion criteria specified by iWITH resulted in the enrollment of a homogeneous cohort characterized by clinical stability and consistently normal liver tests. Moreover, all subjects necessarily came from participating clinical sites, 12 large volume and mature pediatric liver transplant centers specifically selected for experience and infrastructure to conduct a complex clinical trial. Therefore, our study cohort can arguably be described as "clinically ideal" and not representative of the general population of pediatric liver transplant recipients. This context, however, may ironically increase the importance of our findings. It is highly likely that our study, underestimates the prevalence of cluster 1 and overestimates the prevalence of cluster 3 in the general population. Second, our study's cross-sectional design does not shed any light on the evolution of the observed histopathological changes either prior to or, perhaps more importantly, since the time point studied. It is now critically important to determine if the necroinflammatory changes characteristic of cluster 1 translate into progressive fibrosis that can shorten allograft longevity. Our well-characterized cohort provides the foundation for a future longitudinal study based on sequential biospecimens. Third, the inclusion of deceased donor recipients lacking high resolution donor HLA typing data limited the fidelity of the DSA dataset. The deficits are mitigated, at least in part, by the overall harmony of our results with the literature regarding associations between class II DSA and chronic inflammatory allograft damage.[13, 19-23, 28, 42-46]

In summary, our data offers a plausible rationale for the chronic, inflammatory changes that have been repeatedly described but not explained in apparently stable, long-term pediatric liver allografts.[12-18] We show, at the molecular level, interface activity connotes subclinical rejection. Our findings highlight that consistently normal results of liver tests may hide a spectrum of histopathology that can only be

accurately exposed by tissue examination and support the necessity of liver biopsy to guide personalized immunosuppression decision-making.[49] For patients whose biopsies harbor neither inflammation nor fibrosis, immunosuppression dose reduction may be reasonable, based on the consistently reported safety of attempted immunosuppression withdrawal.[8, 9, 50] For patients whose biopsies show fibrosis in the absence of inflammation, our data does not support any recommendations. Lastly, for patients whose biopsies show interface hepatitis, our data indicates that dose reduction may be unwise. Although the intuitive response may be to escalate immunosuppression, data evidencing the benefit of this approach is lacking. Clearly, the next steps are to delineate the natural history of the histopathological phenotypes that we have described which will then inform the design and justify the testing of targeted interventions to optimize allograft health and longevity.

FIGURE LEGENDS

Figure 1: Selection of 157 study participants

Figure 2: Key histological features of 157 biopsies

(A) Heat map and (B) frequencies of histological features.

Figure 3: 157 biopsies divide into three histological clusters

The three variables defining the clusters are Ishak fibrosis stage, interface activity and perivenular fibrosis.

(A) Three-dimensional bubble plot: Bubble size is proportional to the number of observations at that coordinate.

(B) Constellation plot: Each subject is represented by a color-outlined point. Line lengths represent distances between clusters and points. Axis scales are relative distance measures.

Figure 4: Counts of antigen-presenting cells, leukocytes, and APC-leukocyte pairings in virtual antigen-presenting foci

A) H&E section (left) and multiplex Qdot immunostaining of CD34/CD45/class II panel (right) illustrating a "virtual antigen-presenting foci" localized primarily to portal tracts (yellow circles)

B) High magnification (white box, Panel A) of an antigen-presenting focus within a portal tract illustrating CD34+ portal capillaries in the left panel (green), CD45+(high) leukocytes in the middle panel (teal), and a pairing of a CD34-/CD45-/class II+ APC (red) and a CD34-CD45+(high)/class II-(teal)/CD34-/CD45+(high)/ class II+ leukocyte (white) pairing in the right panel. The small white circle in the right panel identifies the APC-leukocyte pairing.

C) Statistical pairwise comparison of clusters for total APCs (CD34-/CD45-/class II+; red cells; upper panel), total leukocytes (CD34-/CD45^{+}/class II +/-; white or teal cells; middle panel), and APC-leukocyte pairings (lower panel).

Figure 5: Microarray transcriptional analysis of liver biopsy samples shows that cluster 1 is enriched in rejection-associated molecular pathways

(A) Weighted gene co-expression network analysis of the liver transcriptome: X-axis: external traits of interest; Y-axis: 33 identified gene modules. The color intensity is proportional to the magnitude of the Pearson correlation coefficient. Asterisks denote statistical significance at p value <0.01. The black arrow signals the selected "salmon" 194-gene module (Supplementary Table 5).

(B) Gene-pathway association network visualizing the relationships between the top 10 KEGG pathways and core genes significantly enriched in the 194-gene "salmon" module. The size of the circled pathways reflects the associated p values of the terms: more significant pathways are larger.

(C) Scatter plot and best-fit line showing the correlation between the scaled sum of the normalized expression levels of the 194 genes of the "salmon" module and the LAFSc. Dots represent individual samples and their color the cluster assignment. *r* corresponds to the Pearson correlation coefficient.

(D) Quantile-quantile plots of expected versus observed scores comparing the distribution of microarray gene expression values for clusters 1, 2, and 3. Differentially expressed genes as computed by the SAM package deviate from the diagonal. Up-regulated versus down-regulated genes at FDR<5% are red open circles in the upper right versus green open circles in the lower left.

(E) CI plot displaying the mean and 95% CI of the activity (log2ratio) of each transplantation-related gene set of interest plotted and color-coded according to their FDR-corrected p values.

REFERENCES

1. Campbell KM, Yazigi N, Ryckman FC, et al. High prevalence of renal dysfunction in long-term survivors after pediatric liver transplantation. J Pediatr 2006;148:475-80.
2. Hathout E, Alonso E, Anand R, et al. Post-transplant diabetes mellitus in pediatric liver transplantation. Pediatr Transplant 2009;13:599-605.
3. Shepherd RW, Turmelle Y, Nadler M, et al. Risk factors for rejection and infection in pediatric liver transplantation. Am J Transplant 2008;8:396-403.
4. Soltys KA, Mazariegos GV, Squires RH, et al. Late graft loss or death in pediatric liver transplantation: an analysis of the SPLIT database. Am J Transplant 2007;7:2165-71.
5. Yanik EL SJ, Shiels MS, et al. Cancer Risk After Pediatric Solid Organ Transplantation. Pediatrics 2017;5:139.
6. Ng VL, Alonso EM, Bucuvalas JC, et al. Health status of children alive 10 years after pediatric liver transplantation performed in the US and Canada: report of the studies of pediatric liver transplantation experience. J Pediatr 2012;160:820-6 e3.
7. Laryea M, Watt KD, Molinari M, et al. Metabolic syndrome in liver transplant recipients: prevalence and association with major vascular events. Liver Transpl 2007;13:1109-14.
8. Benitez C, Londono MC, Miquel R, et al. Prospective multicenter clinical trial of immunosuppressive drug withdrawal in stable adult liver transplant recipients. Hepatology 2013;58:1824-35.
9. Feng S, Ekong UD, Lobritto SJ, et al. Complete immunosuppression withdrawal and subsequent allograft function among pediatric recipients of parental living donor liver transplants. JAMA 2012;307:283-93.

10. Kelly D, Verkade HJ, Rajanayagam J, et al. Late graft hepatitis and fibrosis in pediatric liver allograft recipients: Current concepts and future developments. Liver Transpl 2016;22:1593-1602.

11. Feng S, Bucuvalas J. Tolerance after liver transplantation: Where are we? Liver Transpl 2017;23:1601-1614.

12. Ekong UD, Melin-Aldana H, Seshadri R, et al. Graft histology characteristics in long-term survivors of pediatric liver transplantation. Liver Transpl 2008;14:1582-7.

13. Evans HM, Kelly DA, McKiernan PJ, et al. Progressive histological damage in liver allografts following pediatric liver transplantation. Hepatology 2006;43:1109-17.

14. Herzog D, Soglio DB, Fournet JC, et al. Interface hepatitis is associated with a high incidence of late graft fibrosis in a group of tightly monitored pediatric orthotopic liver transplantation patients. Liver Transpl 2008;14:946-55.

15. Scheenstra R, Peeters PM, Verkade HJ, et al. Graft fibrosis after pediatric liver transplantation: ten years of follow-up. Hepatology 2009;49:880-6.

16. Venturi C, Sempoux C, Quinones JA, et al. Dynamics of allograft fibrosis in pediatric liver transplantation. Am J Transplant 2014;14:1648-56.

17. Syn WK, Nightingale P, Gunson B, et al. Natural history of unexplained chronic hepatitis after liver transplantation. Liver Transpl 2007;13:984-9.

18. Briem-Richter A, Ganschow R, Sornsakrin M, et al. Liver allograft pathology in healthy pediatric liver transplant recipients. Pediatr Transplant 2013;17:543-9.

19. Pongpaibul A, Venick RS, McDiarmid SV, et al. Histopathology of de novo autoimmune hepatitis. Liver Transpl 2012;18:811-8.

20. Ohe H, Uchida Y, Yoshizawa A, et al. Association of anti-human leukocyte antigen and anti-angiotensin II type 1 receptor antibodies with liver allograft fibrosis after immunosuppression withdrawal. Transplantation 2014;98:1105-11.

21. Venturi C, Sempoux C, Bueno J, et al. Novel histologic scoring system for long-term allograft fibrosis after liver transplantation in children. Am J Transplant 2012;12:2986-96.

22. Miyagawa-Hayashino A, Yoshizawa A, Uchida Y, et al. Progressive graft fibrosis and donor-specific human leukocyte antigen antibodies in pediatric late liver allografts. Liver Transpl 2012;18:1333-42.

23. Wozniak LJ, Hickey MJ, Venick RS, et al. Donor-specific HLA Antibodies Are Associated With Late Allograft Dysfunction After Pediatric Liver Transplantation. Transplantation 2015;99:1416-22.

24. O'Leary JG, Demetris AJ, Philippe A, et al. Non-HLA Antibodies Impact on C4d Staining, Stellate Cell Activation and Fibrosis in Liver Allografts. Transplantation 2017;101:2399-2409.

25. Isse K, Lesniak A, Grama K, et al. Preexisting epithelial diversity in normal human livers: a tissue-tethered cytometric analysis in portal/periportal epithelial cells. Hepatology 2013;57:1632-43.

26. Tusher VG, Tibshirani R, Chu G. Significance analysis of microarrays applied to the ionizing radiation response. Proc Natl Acad Sci U S A 2001;98:5116-21.

27. Langfelder P, Horvath S. WGCNA: an R package for weighted correlation network analysis. BMC Bioinformatics 2008;9:559.

28. O'Leary JG, Demetris AJ, Friedman LS, et al. The role of donor-specific HLA alloantibodies in liver transplantation. Am J Transplant 2014;14:779-87.

29. Grabhorn E, Binder TM, Obrecht D, et al. Long-term Clinical Relevance of De Novo Donor-Specific Antibodies After Pediatric Liver Transplantation. Transplantation 2015;99:1876-81.

30. Taner T, Stegall MD, Heimbach JK. Antibody-mediated rejection in liver transplantation: current controversies and future directions. Liver Transpl 2014;20:514-27.

31. Demetris AJ, Bellamy C, Hubscher SG, et al. 2016 Comprehensive Update of the Banff Working Group on Liver Allograft Pathology: Introduction of Antibody-Mediated Rejection. Am J Transplant 2016;16:2816-2835.

32. Troxell ML, Higgins JP, Kambham N. Evaluation of C4d staining in liver and small intestine allografts. Arch Pathol Lab Med 2006;130:1489-96.

33. Bonaccorsi-Riani E, Pennycuick A, Londono MC, et al. Molecular Characterization of Acute Cellular Rejection Occurring During Intentional Immunosuppression Withdrawal in Liver Transplantation. Am J Transplant 2016;16:484-96.

34. Spivey TL, Uccellini L, Ascierto ML, et al. Gene expression profiling in acute allograft rejection: challenging the immunologic constant of rejection hypothesis. J Transl Med 2011;9:174.

35. Halloran PF, Venner JM, Madill-Thomsen KS, et al. Review: The transcripts associated with organ allograft rejection. Am J Transplant 2017.

36. Zhang DY, Goossens N, Guo J, et al. A hepatic stellate cell gene expression signature associated with outcomes in hepatitis C cirrhosis and hepatocellular carcinoma after curative resection. Gut 2016;65:1754-64.

37. Pham MX, Teuteberg JJ, Kfoury AG, et al. Gene-expression profiling for rejection surveillance after cardiac transplantation. N Engl J Med 2010;362:1890-900.

38. Haas M. The Revised (2013) Banff Classification for Antibody-Mediated Rejection of Renal Allografts: Update, Difficulties, and Future Considerations. Am J Transplant 2016;16:1352-7.

39. Haas M. Simultaneous liver-kidney transplantation: shifting renal allograft gene expression from inflammation toward preservation. Kidney Int 2017;91:1010-1013.

40. Burns AM, Chong AS. Alloantibodies prevent the induction of transplantation tolerance by enhancing alloreactive T cell priming. J Immunol 2011;186:214-21.

41. Shiu KY, McLaughlin L, Rebollo-Mesa I, et al. Graft dysfunction in chronic antibody-mediated rejection correlates with B-cell-dependent indirect antidonor alloresponses and autocrine regulation of interferon-gamma production by Th1 cells. Kidney Int 2017;91:477-492.

42. Kaneku H, O'Leary JG, Banuelos N, et al. De novo donor-specific HLA antibodies decrease patient and graft survival in liver transplant recipients. Am J Transplant 2013;13:1541-8.

43. O'Leary JG, Kaneku H, Banuelos N, et al. Impact of IgG3 subclass and C1q-fixing donor-specific HLA alloantibodies on rejection and survival in liver transplantation. Am J Transplant 2015;15:1003-13.

44. Loupy A, Lefaucheur C, Vernerey D, et al. Complement-binding anti-HLA antibodies and kidney-allograft survival. N Engl J Med 2013;369:1215-26.

45. Wiebe C, Gibson IW, Blydt-Hansen TD, et al. Evolution and clinical pathologic correlations of de novo donor-specific HLA antibody post kidney transplant. Am J Transplant 2012;12:1157-67.

46. Chih S, Chruscinski A, Ross HJ, et al. Antibody-mediated rejection: an evolving entity in heart transplantation. J Transplant 2012;2012:210210.

47. O'Leary JG, Kaneku H, Susskind BM, et al. High mean fluorescence intensity donor-specific anti-HLA antibodies associated with chronic rejection Postliver transplant. Am J Transplant 2011;11:1868-76.

48. Kaneku H, O'Leary JG, Taniguchi M, et al. Donor-specific human leukocyte antigen antibodies of the immunoglobulin G3 subclass are associated with chronic rejection and graft loss after liver transplantation. Liver Transpl 2012;18:984-92.

49. Banff Working Group on Liver Allograft P. Importance of liver biopsy findings in immunosuppression management: biopsy monitoring and working criteria for patients with operational tolerance. Liver Transpl 2012;18:1154-70.

50. Feng S, Demetris AJ, Spain KM, et al. Five-year histological and serological follow-up of operationally tolerant pediatric liver transplant recipients enrolled in WISP-R. Hepatology 2017;65:647-660.

Table 1: Characteristics of 157 subjects undergoing iWITH eligibility biopsy

Characteristic*				
Donor	**Age** (years)			15.7 (15.44)
	Male gender			81 (51.6)
	Race (n=132)	White		105 (79.5)
		Black		19 (14.4)
		Other		8 (6.1)
	Deceased			110 (70.1)
Recipient	**Age at transplant** (years)			1.8 (1.70)
	Male gender			79 (50.3)
	Race (n=152)	White		128 (84.2)
		Black		11 (7.2)
		Other		13 (8.6)
	Transplant indication	Acute Liver Failure		11 (7.0)
		Biliary Atresia		86 (54.8)
		Tumor		8 (5.1)
		Metabolic Liver Disease		18 (11.5)
		Other		34 (21.7)
Transplant	**Whole graft**			73 (46.5)
	Previous rejection episodes	0		96 (61.1)
		1		40 (25.5)
		2 or more		21 (13.4)
	Time since last rejection (years)			7.3 (3.22)
At Study Entry	**Age** (years)			10.7 (3.50)
	Time since transplant (years)			8.9 (3.46)
	ALT (U/L)			27.6 (14.57)
	GGT (U/L)			17.4 (7.93)
	Quantitative IgG (n=125; mg/dL)			701.0 (194.95)
	ANA ≥1:40 (n=133)			34 (25.6)
	ASMA = 1:80 (n=133)			5 (3.8)
	α-AT1R antibody (n=119; U/mL)			35.9 (21.49)
	α-ETAR antibody (n=119; U/mL)			35.2 (21.39)
	Class II DSA positive (n=144; MFI ≥2,000)			80 (55.6)
	Class II DSA (n=80)	Number of DSAs	1	42 (52.5)
			2	28 (35.0)
			3 or more	10 (12.5)
		Maximum MFI >20,000		37 (46.2)
		MFI sum >20,000		45 (56.2)

*Continuous variables are summarized using mean and standard deviation (SD). Categorical variables are summarized by counts and percentages.

Table 2: Clinical and serological factors associated with assignment into cluster 1

Characteristic			Reference	OR	95% CI	P Value
Univariable						
Donor	**Age** (per year)			0.98	0.95-1.01	0.14
	Deceased		Living	4.03	1.33-12.20	0.01
Recipient	**Female**		Male	0.47	0.21-1.04	0.06
	Biliary Atresia		Other	0.42	0.19-0.93	0.03
Transplant	**Whole graft**		Partial graft	1.89	0.87-4.08	0.11
	Whole graft		Living graft	4.06	1.29-12.77	0.02
	Deceased partial graft			3.98	1.14-13.97	0.03
	Induction immunosuppression		None	0.55	0.15-1.99	0.36
Study Entry	**Recipient age** (per year)			0.90	0.81-1.01	0.07
	Time since transplant (per year)			0.88	0.78-0.99	0.03
	ALT (per U/L)			1.06	1.02-1.11	0.009
	GGT (per U/L)			1.02	0.97-1.06	0.51
	ANA ≥ 1:40		Negative	1.62	0.65-4.05	0.30
	ASMA = 1:80		Negative	0.98	0.10-9.15	0.99
	α-AT1R antibody (per U/mL)			1.03	1.01-1.05	0.01
	α-ETAR antibody (per U/mL)			1.03	1.00-1.05	0.02
	Class II DSA	**Positive**	Negative	2.90	1.14-7.34	0.02
		Maximum MFI ≤ 20,000	No class II DSA	1.32	0.41-4.24	0.64
		Maximum MFI > 20,000		5.55	2.00-15.44	0.001
		MFI sum ≤ 20,000	No class II DSA	1.36	0.40-4.64	0.63
		MFI sum > 20,000		4.49	1.67-12.14	0.003
Multivariable						
	ALT (per U/L)			1.07	1.02-1.13	0.01
	Class II DSA	**MFI sum ≤ 20,000**	No class II DSA	1.50	0.43-5.26	0.53
		MFI sum > 20,000		5.11	1.82-14.41	0.002

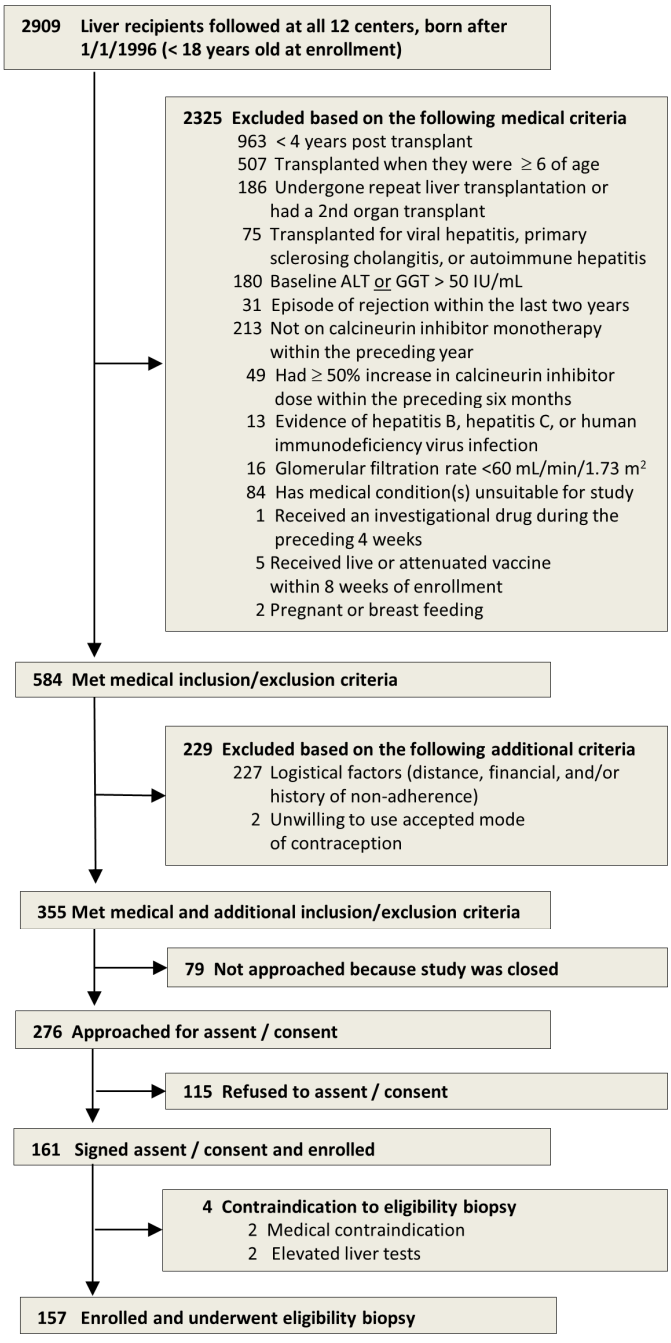
2909 Liver recipients followed at all 12 centers, born after 1/1/1996 (< 18 years old at enrollment)
2325 Excluded based on the following medical criteria
963 < 4 years post transplant
507 Transplanted when they were ≥ 6 of age
186 Undergone repeat liver transplantation or had a 2nd organ transplant
75 Transplanted for viral hepatitis, primary sclerosing cholangitis, or autoimmune hepatitis
180 Baseline ALT or GGT > 50 IU/mL
31 Episode of rejection within the last two years
213 Not on calcineurin inhibitor monotherapy within the preceding year
49 Had ≥ 50% increase in calcineurin inhibitor dose within the preceding six months
13 Evidence of hepatitis B, hepatitis C, or human immunodeficiency virus infection
16 Glomerular filtration rate <60 mL/min/1.73 m²
84 Has medical condition(s) unsuitable for study
1 Received an investigational drug during the preceding 4 weeks
5 Received live or attenuated vaccine within 8 weeks of enrollment
2 Pregnant or breast feeding
584 Met medical inclusion/exclusion criteria
229 Excluded based on the following additional criteria
227 Logistical factors (distance, financial, and/or history of non-adherence)
2 Unwilling to use accepted mode of contraception
355 Met medical and additional inclusion/exclusion criteria
79 Not approached because study was closed
276 Approached for assent / consent
115 Refused to assent / consent
161 Signed assent / consent and enrolled
4 Contraindication to eligibility biopsy
2 Medical contraindication
2 Elevated liver tests
157 Enrolled and underwent eligibility biopsy

A

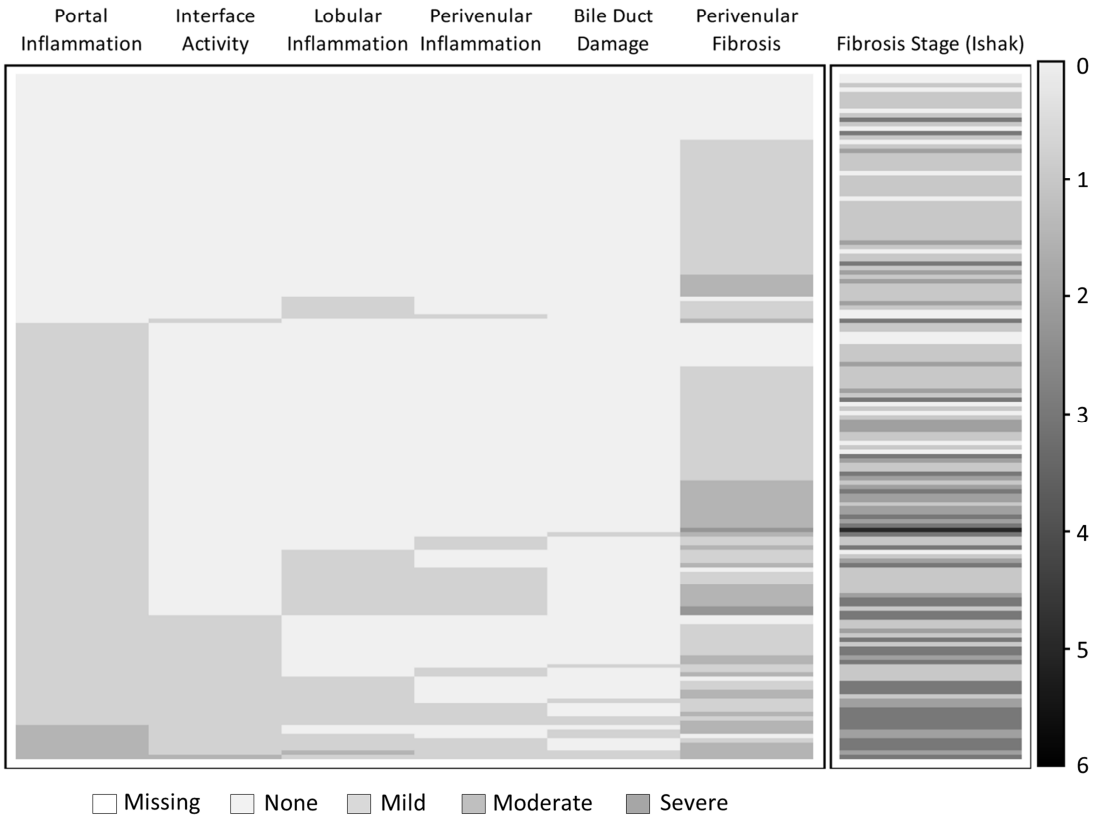

B

	Inflammation				Bile Duct Damage	Peri-venular Fibrosis	Ishak Fibrosis Stage	
N=157	**Portal**	**Interface**	**Lobular**	**Peri-venular**				
None	57 36%	123 78%	120 76%	130 83%	148 94%	31 20%	**0-1**	96 61%
Mild	92 59%	33 21%	36 23%	27 17%	9 6%	85 54%	**2**	27 17%
Moderate	8 5%	1 1%	1 1%	0	0	38 24%	**3**	33 21%
Severe	0	0	0	0	0	3 2%	**4-5**	1 (1%)

A

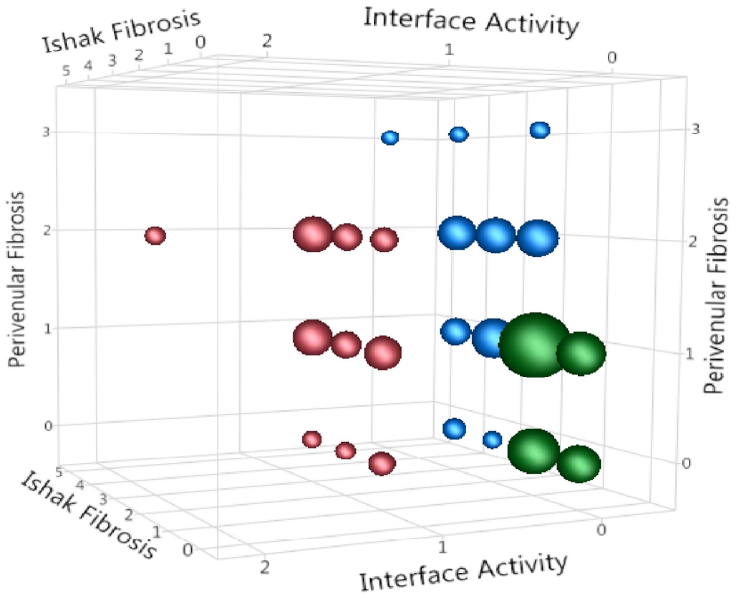

B

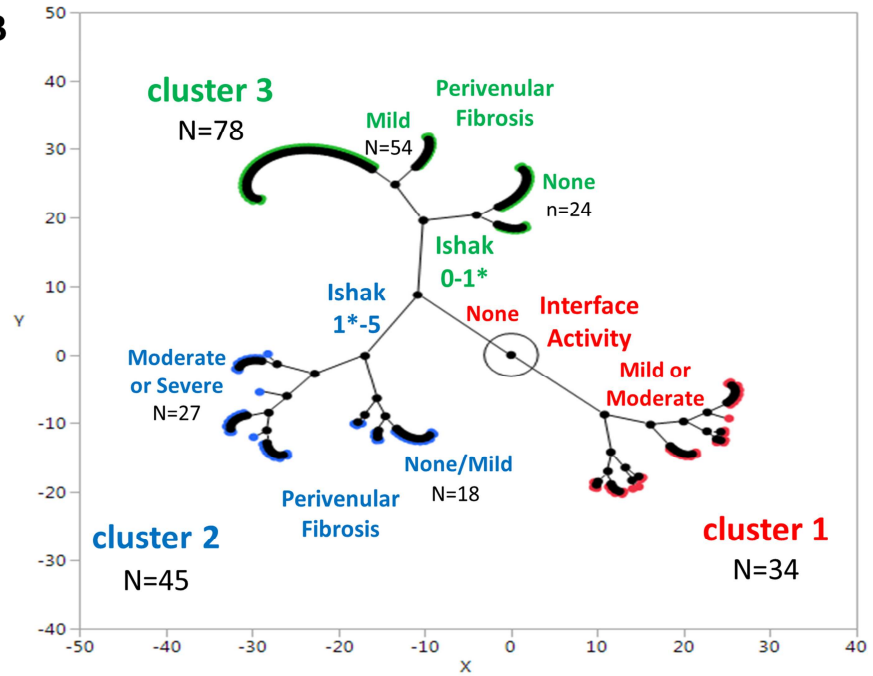

*cluster 1: Ishak 0/1 + Perivenular fibrosis none/mild
cluster 2: Ishak 1 + perivenular fibrosis moderate/severe; Ishak ≥2

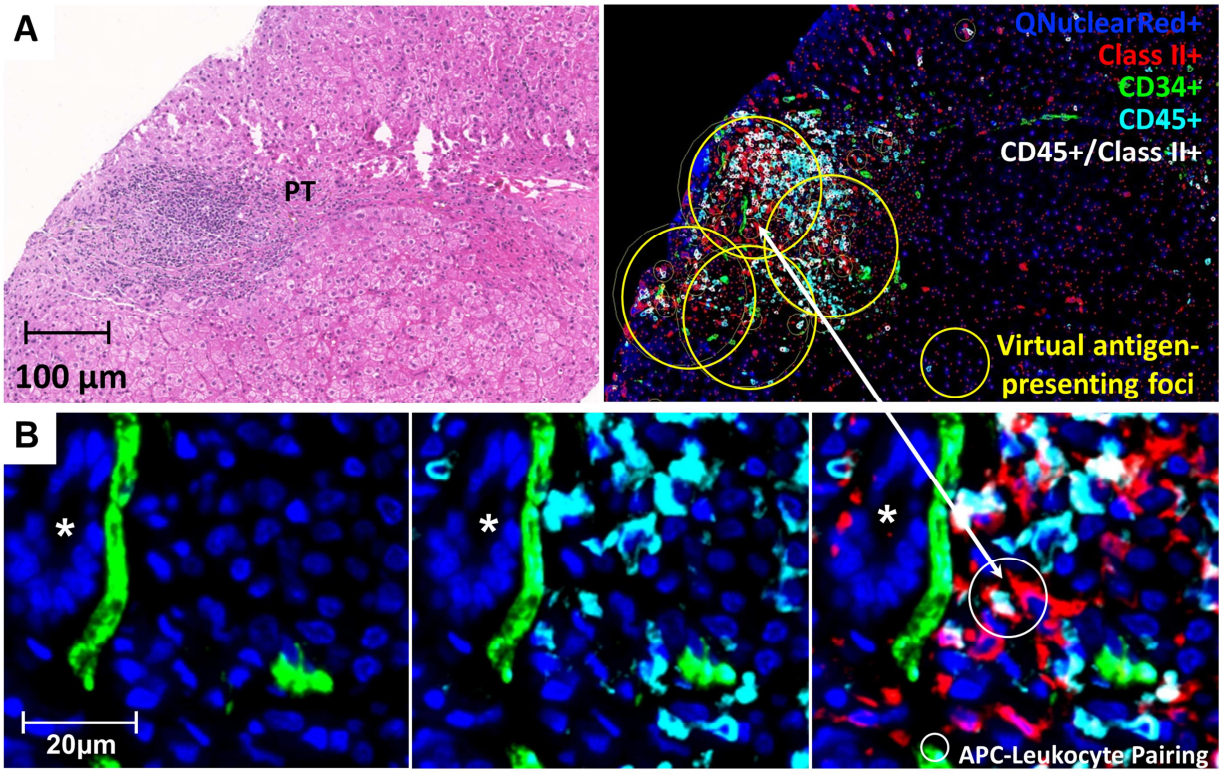

C

CD34-/CD45-/ClassII+ RED = APCs	Comparison	p-value
	cluster 1 vs 2	0.0966
	cluster 1 vs 3	<0.0001
	cluster 2 vs 3	0.0039

CD34-/CD45+/ClassII+/- WHITE or TEAL = leukocytes	Comparison	p-value
	cluster 1 vs 2	<0.0001
	cluster 1 vs 3	<0.0001
	cluster 2 vs 3	0.1625

APC-Leukocyte Pairing RED ← → WHITE or TEAL CELLS	Comparison	p-value
	cluster 1 vs 2	0.0003
	cluster 1 vs 3	<0.0001
	cluster 2 vs 3	0.0329

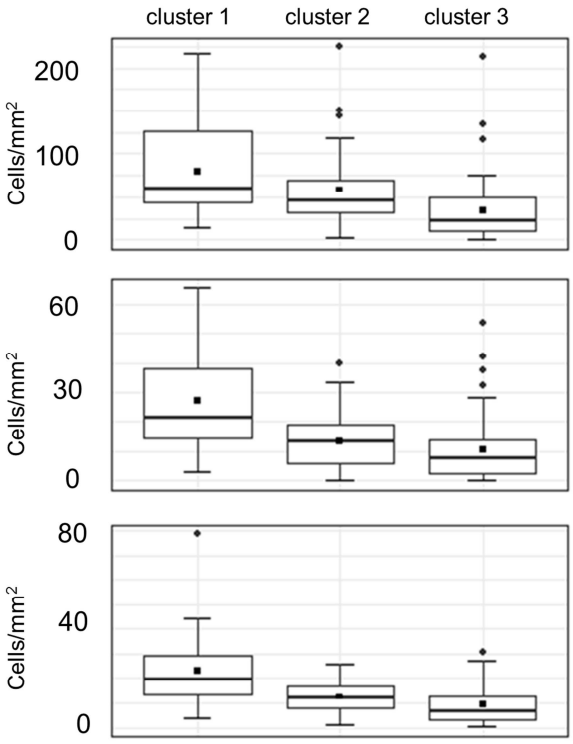

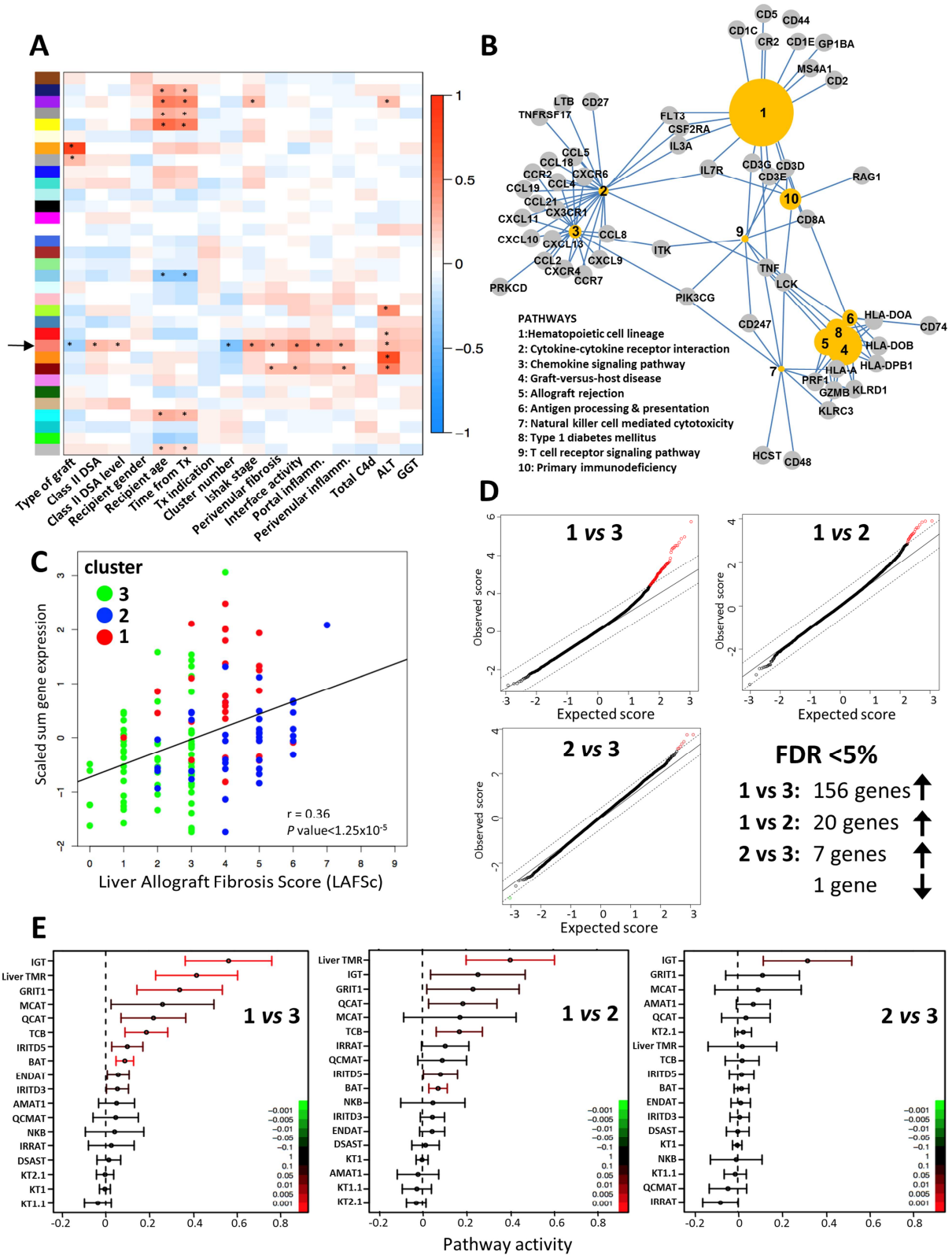
A
Type of graft
Class II DSA
Class II DSA level
Recipient gender
Recipient age
Time from Tx
Tx indication
Cluster number
Ishak stage
Perivenular fibrosis
Interface activity
Portal inflamm.
Perivenular inflamm.
Total C4d
ALT
GGT
1
0.5
0
−0.5
−1
B
PATHWAYS
1:Hematopoietic cell lineage
2: Cytokine-cytokine receptor interaction
3: Chemokine signaling pathway
4: Graft-versus-host disease
5: Allograft rejection
6: Antigen processing & presentation
7: Natural killer cell mediated cytotoxicity
8: Type 1 diabetes mellitus
9: T cell receptor signaling pathway
10: Primary immunodeficiency
C
cluster
3
2
1
Scaled sum gene expression
Liver Allograft Fibrosis Score (LAFSc)
r = 0.36
P value<1.25x10-5
D
1 vs 3
1 vs 2
2 vs 3
Observed score
Expected score
FDR <5%
1 vs 3: 156 genes
1 vs 2: 20 genes
2 vs 3: 7 genes
1 gene
E
1 vs 3
1 vs 2
2 vs 3
Pathway activity

Supplementary Methods

Routine Histology, C4d Scoring, Multiplex Quantum Dot (Qdot®) Immunolabeling, and Automated Image Analysis

Batched slide sets (34 maximum per batch) were multiplex-stained at room temperature on a LabVision Autostainer 360, followed by Qnuclear™ Deep Red Stain (Q10363, ThermoFisher/Invitrogen, Carlsbad, CA), dehydration through alcohols and xylenes and coverslipping utilizing EcoMount (EM897L, Biocare Medical, Pacheco, CA), as previously described[1]. Briefly, primary antibody labeling (Table below) was followed by i) PBS-T washing, ii) detection using an appropriate biotinylated IgG secondary antibody (BA-1000 or BA-2000, Vector Labs, Burlingame, CA), and iii) streptavidin conjugated Qdot® labeling (605: Q10101MP; 655: Q10121MP; 705: Q10161MP; 800: Q10171MP; Molecular Probes, Eugene, OR). Blocking was performed between primary antibody applications using Avidin/Biotin Blocking Kit (SP-2001, Vector Labs, Burlingame, CA) and Serum-Free Protein Block (X090930-2, Agilent/Dako, Santa Clara, CA).

Primary Antibodies

Antigen	Company (catalog #)	Dilution (into PBS)	1st incubation time	Qdot	Qdot Dilution	2nd incubation time
Mouse α-human CD34	Dako (M7165)	1:100	4 HR	605 or 705	1:50 or 1:250	30 min
Mouse α-human CD45	Dako (M0701)	1:500	2 HR	705	1:250	30 min
Rabbit α-human MHCII	Abcam (ab157210)	1:1000	2 HR	800	1:500	30 min
Mouse α-human Ki-67 (MIB-1)	Dako (M7240)	1:100	4 HR	705	1:50	30 min
Mouse α-human SMA	Dako (M0851)	1:2000	2 HR	800	1:500	30 min

A Zeiss AxioScan Z.1 (Carl Zeiss, Jena, Germany) setup using a 20x/0.8NA objective, cooled 16-bit sCMOS camera (Hamamatsu Photonics, Hamamatsu City, Japan), and HXP-120V metal halide excitation source created the multiplex WSI. Filter sets appropriately matched each fluorophore/Qdot® to maximize the emission spectra signal to noise ratio (Semrock, Rochester, NY; Omega, Brattleboro, VT; Chroma,

Bellows Falls, VT). Pixel-based quantitative morphometry of trichrome-stained slides calculated the total tissue biopsy percentage occupied by fibrosis. All WSIs were checked for folds, focus quality, and optimized staining; suboptimal areas were discarded. Fully automated tissue-tethered cytometry was then performed using internally developed image analysis software (NearCYTE; http://nearcyte.org) that co-localizes multiple analytes via a defined nuclear marker and parametric segmentation. Multiplex staining panels included: a) CD34/SMA/Ki-67 (MIB-1) for sinusoidal capillarization, stellate cell activation, and proliferating cells (Supplementary Figure 2); and b) HLA class II/CD34/CD45 for extent of class II expression, antigen presenting cells (APCs), and total leukocyte load. Only CD45 (high) cells (predominantly lymphocytes)[2] were considered CD45+ and included in the automated morphometric analyses. Analyte expression patterns were defined via morphological parameters, such as staining intensity, circumferential expansion of the segmented nuclear edges to define cytoplasmic areas, and threshold of signal expression per area (nuclear versus cytoplasmic) needed to define "positive" classifications. Defined expression patterns were then applied via automated batch processing across all slides without human intervention. Classification results were then reviewed as a WSI overlay and/or via generated summary statistics. Following WSI classification, additional spatial-based reporting logic was incorporated for pattern discovery (e.g. clustering of known cell phenotypes, structural distances, and other spatial characteristics. For example, "virtual antigen-presenting foci" were defined as circular areas (diameter of 100 microns) centered on density-based spatial clusters (DBSCAN, radius=15 microns) of ≥5 CD34-/CD45-/class II+ cells, most of which are dendritic cells or monocytes/macrophages. Visual inspection of five non-systematically selected biopsies from each cluster showed that the vast majority (>85%) of virtual antigen-presenting foci, as expected, overlapped with portal/periportal areas. The remaining foci were located mostly in perivenular and rarely in mid-lobular areas. An "APC-leukocyte pairing" was defined as a CD34-/CD45-/class II+ cell (APC) located within 5 microns of a CD34-/CD45-/class II+/-cell (leukocyte).

Liver tissue gene expression experiments

RNA samples (n=151) were extracted from cryopreserved liver tissue samples using TRIzol and hybridized onto Affymetrix Human Genome U219 96-array plates (Thermo Fisher Scientific, High Wycombe, United Kingdom). We performed quality control using AffyPLM[3] and excluded samples with a *Normalized Unscaled Standard Error* >1.05, resulting in 133 evaluable arrays. Raw expression data were normalized using the robust multi-array algorithm[4] with a custom probe set definition that mapped probes to Entrez Gene IDs[5]. To eliminate genes with invariant expression levels, only those with a *coefficient* of *variation* ≥0.034 across all microarrays were considered for downstream analysis. We used *Significant Analysis of Microarray*[6] and conducted 1,000 data permutations to identify differentially expressed genes and to estimate the False Discovery Rate (FDR). Differential gene expression was also assessed using linear models and empirical Bayes moderated t-statistics (*Linear Models for Microarray Analysis*, LIMMA; R-package software)[7] with FDRs computed using the Benjamini-Hochberg procedure. We employed the *Weighted Gene Correlation Network Analysis* package available from R[8] to identify modules of co-expressed genes highly correlated with external demographic, clinical, serological and histological traits. Applying a power adjacency function β=4 to the absolute Pearson correlation matrices, we identified 33 distinct co-expression modules containing from 31 to 5,248 genes each.

Validation gene expression experiments on 148 RNA samples were conducted using the Nanostring nCounter platform and a pre-defined *PanCancer Immune Profiling Panel* containing 770 genes to which we added 30 additional genes, selected on the basis of their previously described involvement in rejection, stellate cell function and liver fibrosis. Raw data were normalized using the NanoStringNorm package[9] [R using the geometric mean of the most stable genes (*MTMR14, CNOT10, MRPS5, EIF2B4, SF3A3, TLK2*)]. Differential expression was assessed using the LIMMA package described above. The statistical significance of *a priori* defined sets of genes representing biological pathways on the microarray-derived expression dataset was computed employing *Quantitative Set Analysis for Gene Expression* (QuSAGE)[10],

using the transplantation-related *Pathogenesis-Based Transcript* gene sets from the Alberta Transplant Applied Genomics Centre (ATAGC; http://atagc.med.ualberta.ca/Research/GeneLists) together with a 13-gene signature (*CCL19, SLC1A3, HMMR, GPNMB, CXCL9, GBP2, HLA-DMA, MMP9, MMP7, TOP2A, PLA2G7, FABP5, CD74*) previously described as highly specific for T cell mediated rejection in stable liver recipients undergoing immunosuppression withdrawal.[11] To compare the over-representation of biological pathways in clusters 1, 2 and 3, we employed Gene Set Enrichment Analysis (GSEA)[12] and gene sets derived from the *Kyoto Encyclopedia of Genes and Genomes* (KEGG) and Hallmark pathway databases available from the Molecular Signatures Database. GSEA analyses were performed using the GSEAPreranked tool, based on t-statistic and a weighted scoring scheme with 1,000 permutations. To identify KEGG pathways enriched in selected modules of co-expressed genes we employed the *enricher* function from *ClusterProfiler* R-package for hypergeometric tests[13] and used the *cnetplot* method to visualize the gene-pathway association networks[14].

Supplementary Methods References

1. Isse K, Grama K, Abbott IM, et al. Adding value to liver (and allograft) biopsy evaluation using a combination of multiplex quantum dot immunostaining, high-resolution whole-slide digital imaging, and automated image analysis. Clin Liver Dis 2010;14:669-85.
2. Im M, Chae H, Kim T, et al. Comparative quantitative analysis of cluster of differentiation 45 antigen expression on lymphocyte subsets. Korean J Lab Med 2011;31:148-53.
3. Bolstad BM, Collin F, Brettschneider J. Quality Assessment of Affymetrix GeneChip Data. . In: Gentleman R, ed. Bioinformatics and Computational Biology Solutions Using R and Bioconductor. New York: Springer, 2005.
4. Irizarry RA, Bolstad BM, Collin F, et al. Summaries of Affymetrix GeneChip probe level data. Nucleic Acids Res 2003;31:e15.
5. Dai M, Wang P, Boyd AD, et al. Evolving gene/transcript definitions significantly alter the interpretation of GeneChip data. Nucleic Acids Res 2005;33:e175.
6. Tusher VG, Tibshirani R, Chu G. Significance analysis of microarrays applied to the ionizing radiation response. Proc Natl Acad Sci U S A 2001;98:5116-21.
7. Smyth G. Limma: Linear Models for Microarray Data. In: Gentleman R, ed. Bioinformatics and Computational Biology Solutions Using R and Bioconductor. New York: Springer, 2005:397-420.
8. Langfelder P, Horvath S. WGCNA: an R package for weighted correlation network analysis. BMC Bioinformatics 2008;9:559.
9. Waggott D, Chu K, Yin S, et al. NanoStringNorm: an extensible R package for the pre-processing of NanoString mRNA and miRNA data. Bioinformatics 2012;28:1546-8.
10. Yaari G, Bolen CR, Thakar J, et al. Quantitative set analysis for gene expression: a method to quantify gene set differential expression including gene-gene correlations. Nucleic Acids Res 2013;41:e170.

11. Bonaccorsi-Riani E, Pennycuick A, Londono MC, et al. Molecular Characterization of Acute Cellular Rejection Occurring During Intentional Immunosuppression Withdrawal in Liver Transplantation. Am J Transplant 2016;16:484-96.

12. Subramanian A, Tamayo P, Mootha VK, et al. Gene set enrichment analysis: a knowledge-based approach for interpreting genome-wide expression profiles. Proc Natl Acad Sci U S A 2005;102:15545-50.

13. Yu G, Wang LG, Han Y, et al. clusterProfiler: an R package for comparing biological themes among gene clusters. OMICS 2012;16:284-7.

14. Yu G, Wang LG, Yan GR, et al. DOSE: an R/Bioconductor package for disease ontology semantic and enrichment analysis. Bioinformatics 2015;31:608-9.

Supplementary Figure Legends

Supplementary Figure 1: **Multiplex staining and image analysis**

(A) Example of CD34/Ki-67 (MIB-1)/SMA multiplex stain illustrating a small portal tract in the center with a proliferating SMA+/Ki-67 (MIB-1)+ putative periportal stellate cell shown in the lower right inset.

(B) Color deconvolution using pixel area morphometry was used to quantify liver fibrosis, shown over-laid on the original image.

(C) Correlation between LAFSc and Trichrome Area/Total biopsy area.

Supplementary Figures 2A and 2B: C4d scores of 157 eligibility biopsies.

(A) Heat map and (B) frequencies of C4d scores.

Supplementary Figure 3: Autoantibody profiles of enrolled subjects

(A) ANA and ASMA (n=133). Numbers and percentages are shown.

(B) α-AT1R and α-ETAR antibodies (n=119). The threshold defining positive is 17 U/ml.

Supplementary Figure 4: Comparison of class II DSA MFI by cluster

The bar graph shows the proportion of each cluster for each class II DSA MFI value. The numbers shown are absolute numbers.

(A) Maximum detected class II DSA MFI

(B) Sum of class II DSA MFI

Supplementary Figure 5: Nanostring liver biopsy differential gene expression between clusters 1, 2, and 3

Expression profiles of the 109 genes differentially expressed in at least one comparison at p-value <0.05 and fold change >1.5 are expressed as a matrix view of gene expression data where rows represent genes and columns represent hybridized samples. The intensity of each color denotes the standardized ratio between each value and the average expression of each gene across all samples. Red or green colored pixels correspond to an increased or decreased abundance of the mRNA in the indicated sample.

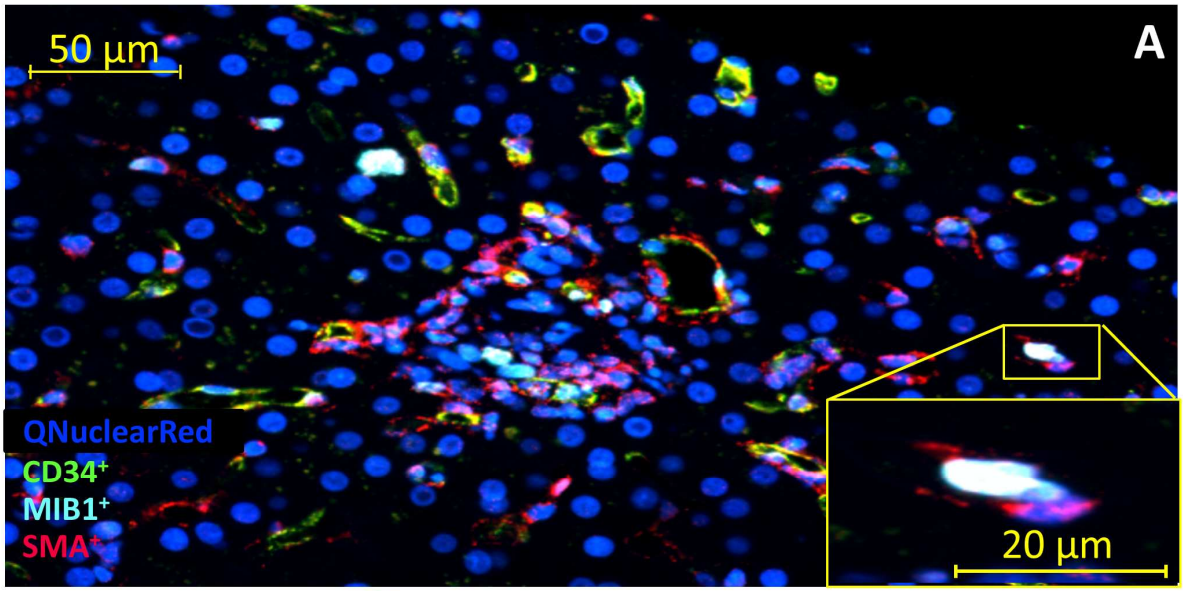
50 µm
A
QNuclearRed
CD34+
MIB1+
SMA+
20 µm

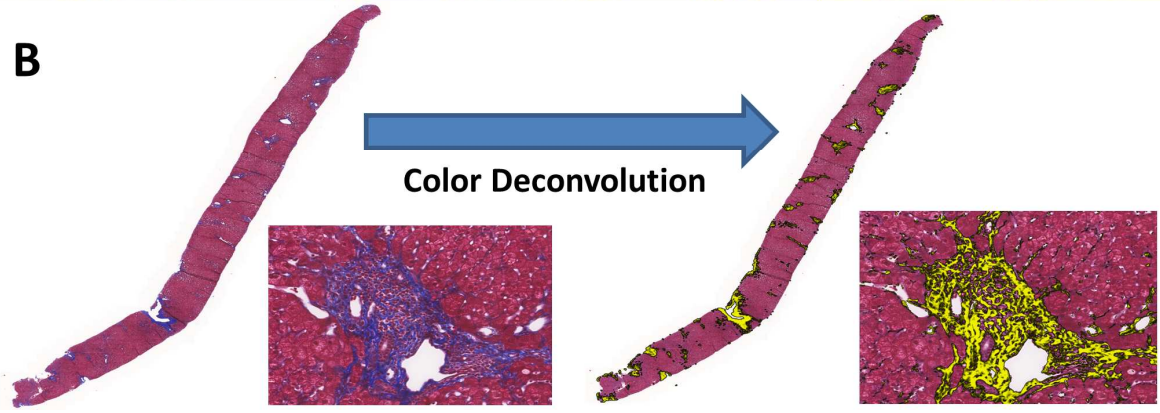
B
Color Deconvolution

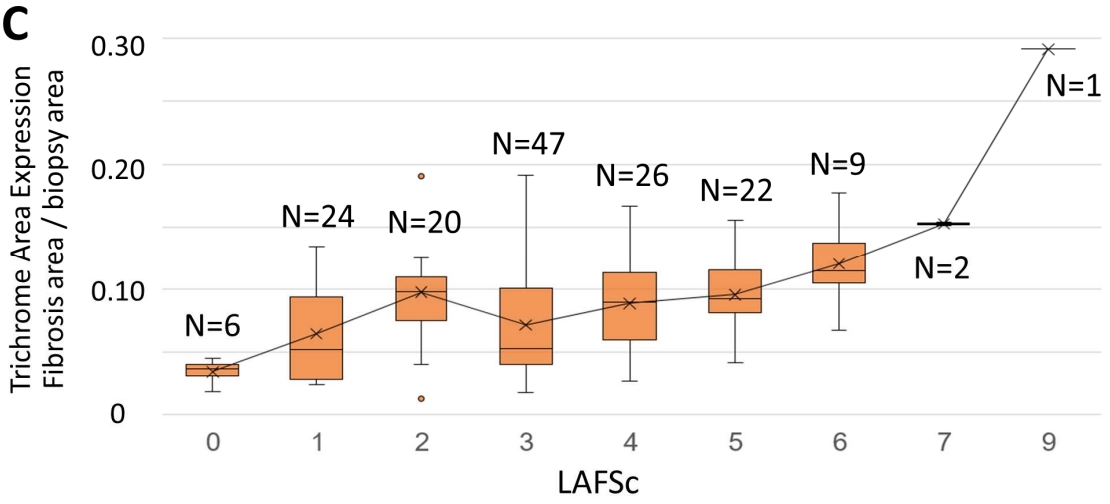
C
Trichrome Area Expression
Fibrosis area / biopsy area
0.30
0.20
0.10
0
N=6
N=24
N=20
N=47
N=26
N=22
N=9
N=2
N=1
0
1
2
3
4
5
6
7
9
LAFSc

A

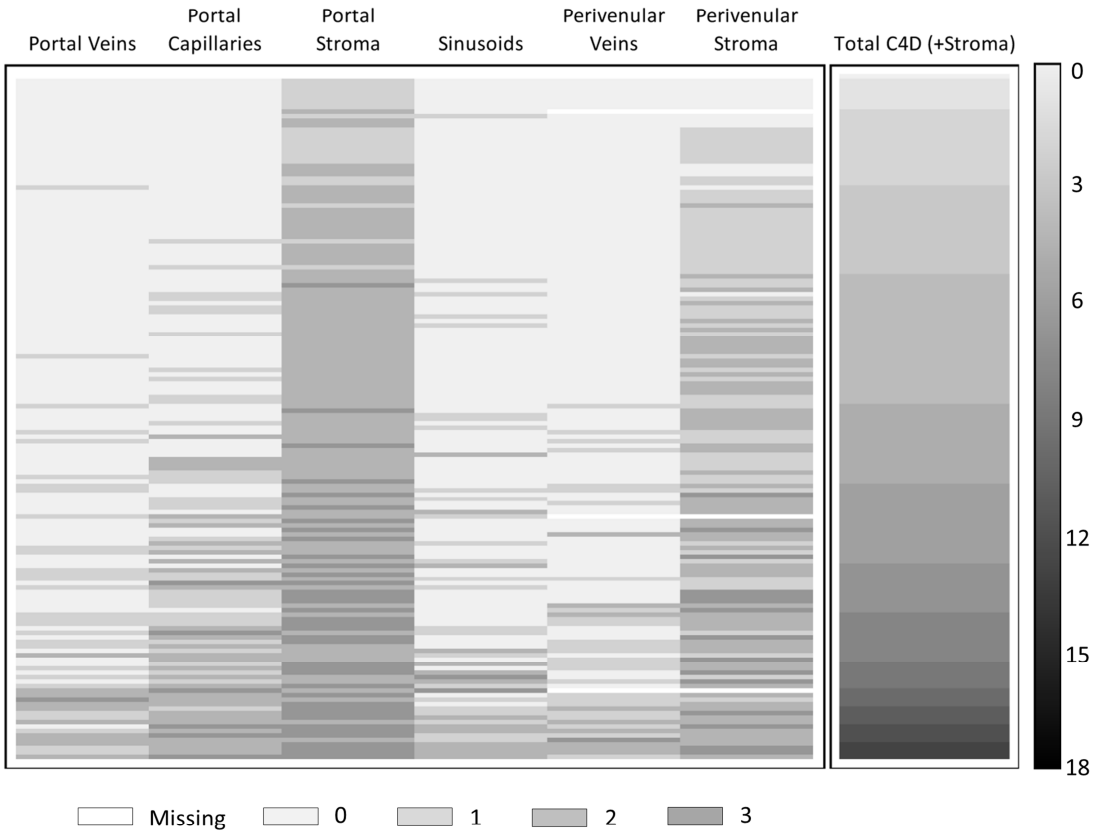

B

Score	Portal (n=153)			Sinusoid (n=153)	Perivenular (n=150)		Total C4d Score (n=154)	
	Veins	Capillaries	Stroma		Veins	Stroma		
0	113 (74%)	81 (53%)	0	112 (73%)	114 (76%)	15 (10%)	**0 - 3**	45 29%
1	29 (19%)	36 (24%)	21 (14%)	25 (16%)	26 (17%)	62 (41%)	**4 - 6**	65 42%
2	10 (7%)	30 (20%)	94 (61%)	14 (9%)	9 (6%)	58 (39%)	**7 - 9**	28 18%
3	1 (1%)	6 (4%)	38 (25%)	2 (1%)	1 (1%)	15 (10%)	**>9**	16 10%

A

N	ANA				ASMA	
	Negative	1:40	1:160	>1:160	Negative	1:80
133	99 (74.4)	17 (12.6)	13 (9.8)	4 (3.0)	128 (96.3)	5 (3.7)

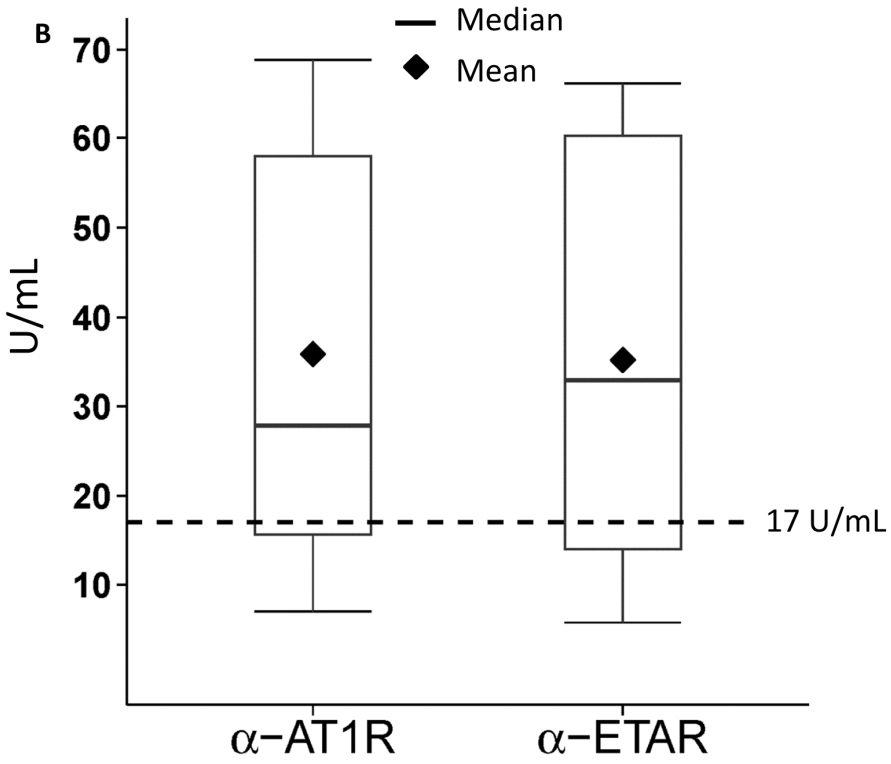

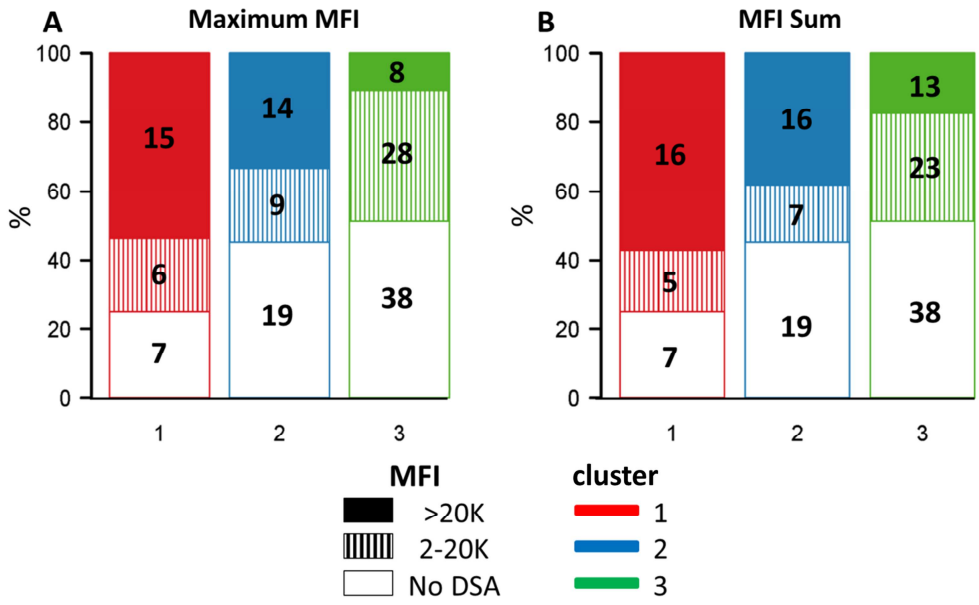
A
Maximum MFI
B
MFI Sum
%
100
80
60
40
20
0
15
6
7
14
9
19
8
28
38
16
5
7
16
7
19
13
23
38
1
2
3
MFI
>20K
2-20K
No DSA
cluster
1
2
3

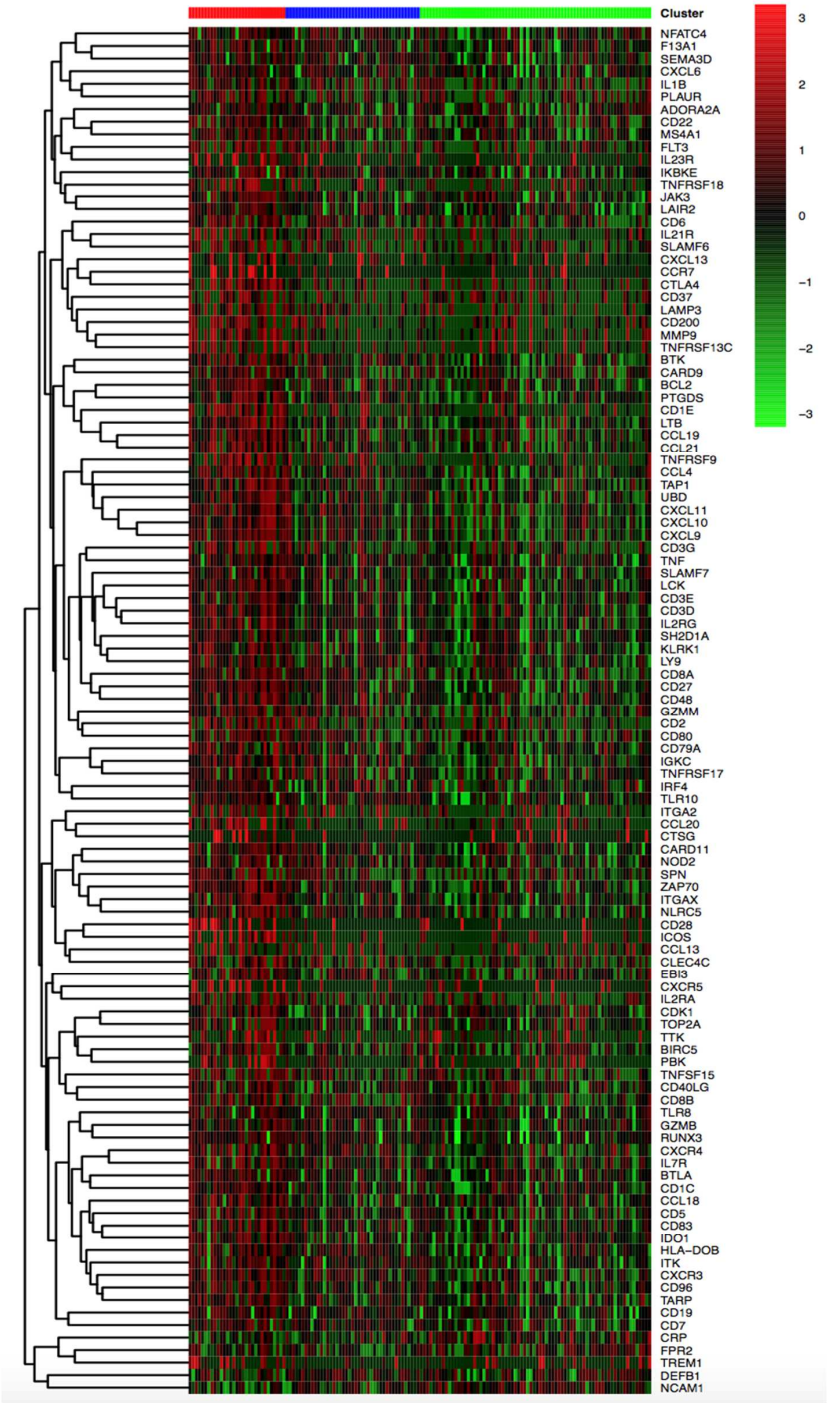
Cluster
3
2
1
0
−1
−2
−3
NFATC4
F13A1
SEMA3D
CXCL6
IL1B
PLAUR
ADORA2A
CD22
MS4A1
FLT3
IL23R
IKBKE
TNFRSF18
JAK3
LAIR2
CD6
IL21R
SLAMF6
CXCL13
CCR7
CTLA4
CD37
LAMP3
CD200
MMP9
TNFRSF13C
BTK
CARD9
BCL2
PTGDS
CD1E
LTB
CCL19
CCL21
TNFRSF9
CCL4
TAP1
UBD
CXCL11
CXCL10
CXCL9
CD3G
TNF
SLAMF7
LCK
CD3E
CD3D
IL2RG
SH2D1A
KLRK1
LY9
CD8A
CD27
CD48
GZMM
CD2
CD80
CD79A
IGKC
TNFRSF17
IRF4
TLR10
ITGA2
CCL20
CTSG
CARD11
NOD2
SPN
ZAP70
ITGAX
NLRC5
CD28
ICOS
CCL13
CLEC4C
EBI3
CXCR5
IL2RA
CDK1
TOP2A
TTK
BIRC5
PBK
TNFSF15
CD40LG
CD8B
TLR8
GZMB
RUNX3
CXCR4
IL7R
BTLA
CD1C
CCL18
CD5
CD83
IDO1
HLA−DOB
ITK
CXCR3
CD96
TARP
CD19
CD7
CRP
FPR2
TREM1
DEFB1
NCAM1